Progress of Theoretical Physics, Vol. 121, No. 2, February 2009

Microscopic Calculation of the Wobbling Excitations Employing the Woods-Saxon Potential as a Nuclear Mean-Field

Takuya SHOJI and Yoshifumi R. SHIMIZU

Department of Physics, Graduate School of Sciences, Kyushu University, Fukuoka 812-8581, Japan

(Received November 28, 2008)

The wobbling excitations of the triaxial superdeformed (TSD) bands in the Lu and Hf region are studied by the microscopic framework of the cranked mean-field and the random-phase approximation (RPA). In contrast to the previous works, where the Nilsson potential was used, the more realistic Woods-Saxon potential is employed as a nuclear mean-field. It is pointed out that the original formulation should be slightly modified for general mean-field like the Woods-Saxon potential. The wobbling-like RPA solutions have been found systematically in the nuclei studied and their characteristic properties are investigated in detail. This confirms the wobbling phonon excitations in TSD nuclei from the microscopic calculations. The result of $B(E2)$ values indicates that the triaxial deformation is increasing as a function of spin in the observed TSD bands in ^{163}Lu.

Subject Index: 210, 211, 212

§1. Introduction

The observation of the wobbling excitations[1),2)] (see also Refs. 3) and 4)) renewed the interest in the study of nuclear rotational motions. The nuclear wobbling motion[5)] is a quantized motion of the triaxial rotor and appears as a multiple-band structure, in which consecutive rotational bands are connected by strong $E2$ transitions with each other. Until now, the multiple rotational band structure characteristic to the wobbling phonon excitation has been observed at the high-spin excited states in some Lu isotopes[1)–3),6)–10)] around ^{163}Lu. Nuclei in the Lu and Hf region, including these Lu isotopes, have been predicted to be strongly deformed with pronounced triaxiality[11)–14)] at high-spin states, and the associated rotational bands are called triaxial superdeformed (TSD) bands; i.e., the wobbling structure is composed of these TSD bands. In fact the lifetime measurements in these nuclei[15),16)] revealed that the rotational $E2$ transition probabilities inside the bands are typically about 500 Weisskopf units, and those between the bands associated with the wobbling phonon excitations are about 100 Weisskopf units. These are one of the largest out-of-band $B(E2)$ and believed to be the evidence of the nuclear wobbling motion. Although several candidates of the TSD bands have been observed in even-even Hf isotopes,[17)–21)] there is no definite evidence of the wobbling excitation yet.

The nuclear wobbling motion was first predicted by using the simple macroscopic rotor model.[5)] The experimental data observed in Lu isotopes are investigated by the particle-rotor model,[22)–25)] because a $i_{13/2}$ quasiproton exists in the proton-odd Lu nuclei. It is, however, noted that the properties of the observed out-of-band $E2$ transitions suggest that the triaxial deformation is of the so-called positive-γ

shape in the Lund convention,[26] the sign of which is opposite to that of Ref. 5); namely the moment of inertia about the shortest axis of triaxial deformation is the largest. This conflicts with the irrotational moments of inertia which are natural for the macroscopic rotor model, where the moment of inertia is largest about the intermediate axis. In principle, the triaxiality for the quadrupole shape and that for the moments of inertia can be taken differently in the macroscopic model; the so-called "γ-reversed" moments of inertia, i.e., those about the shortest and intermediate axes are interchanged, are used in Refs. 22) and 23), while the rigid-body moments of inertia that are consistent with the positive γ shape are recommended in Refs. 24) and 25). Since the moments of inertia are the basic parameters (inputs) of the macroscopic model, microscopic approaches are necessary to investigate this problem.

From the theoretical point of view, how the rotor model emerges out of the collective rotational motions of constituent nucleons is an interesting and long-standing problem (see e.g. Ref. 27)). Most of nuclei are axially-deformed in their ground states and the collective rotation is of one-dimensional nature (rotation about only one axis). In contrast, the wobbling excitations correspond to tilting the main rotation axis from the principal axis of deformation, and the rotation is of three-dimensional nature. Therefore, the microscopic study of the wobbling motion, which is characteristic in the rotor model, is expected to give a new insight to the problem of how the individual nucleons form and affect the triaxial nuclear rotor. The key to relate the motions of nucleons to the collective rotation is the introduction of the "body-fixed" or the principal axis (PA) frame,[28] in which no collective rotations exist. The condition of the body-fixed frame defines the constraints to the many-body system, and combined with the redundant rotor degrees of freedom the original many-body problem is recovered. The idea of this "collective coordinate method" in quantum many-body systems was put forward in Ref. 29), especially for the nuclear triaxial rotor problem in Refs. 30) and 31). The rigorous quantum mechanical treatment of the constraints is a difficult problem, but Marshalek showed[32] by taking the small amplitude limit of the time-dependent HFB (TDHFB) theory that the transformation to the PA frame is straightforward within the order of the random-phase approximation (RPA), see also Refs. 33) and 34). The semiclassical treatment of the collective rotational motion based on the TDHFB theory was developed in Refs. 35) and 36), in which the PA frame constraints are taken into account properly. The attempts to go beyond the RPA order have been done[37),38] based on the selfconsistent-collective coordinate method.[39),40]

In Marshalek's theory,[32] it has been shown that the RPA eigenenergy can be written in the same form as the wobbling phonon energy in terms of the three moments of inertia, which can be derived either in the classical asymmetric top[41] or in its quantum analogy, the triaxial rotor model,[5] by using the small amplitude assumption consistent to the RPA. It has been also shown[42] that the $E2$ transition probabilities associated with the wobbling excitation can be written in the same way as in the rotor model[5] if the RPA eigenmode has a certain property. It should, however, be stressed that the actual calculations are performed in the cranked mean-field plus RPA approach,[43)–45] which is formulated in the uniformly rotating (UR)

frame according to the usual cranking prescription. It is the introduction of the PA frame and the transformation from the UR to PA frame that makes it possible to interpret a microscopic RPA eigenmode as the wobbling phonon and to derive the three moments of inertia of the rotor microscopically. In the theory of Ref. 32) as well as those in Refs. 35) and 38), the PA frame is defined such that the non-diagonal part of the (mass) quadrupole tensor should vanish identically.[28] It is discussed in Refs. 29) and 31) that the PA frame condition is a gauge fixing condition and physical observables should not depend on its choice; for example, the three moments of inertia in the PA (body-fixed) frame themselves are gauge-dependent and are not the physical observables. However, in order to obtain a clear physical picture and a relation to the macroscopic rotor model, the introduction of the specific PA frame condition corresponding to the nuclear rotor is important and useful.

According to Marshalek's wobbling theory, microscopic RPA calculations have been performed for nuclei in the Hf and Lu region,[46)–48)] where it was found that the RPA eigenmode that can be interpreted as the wobbling phonon exists in each nucleus stably in a reasonable range of mean-field deformations (see also Ref. 49)). Although it is not confirmed in experiment, the possible wobbling excitations in normal deformed nuclei with the negative-γ shapes have been also studied previously[42),50)] and more recently.[51] The relation between the instability of the wobbling RPA mode and the appearance of the tilted axis cranking[52] mean-field solution is also discussed.[49),53),54)] In the previous calculations,[46)–48)] the calculated out-of-band to in-band $B(E2)$ ratio was systematically smaller by about factor two than the experimental data, but it was shown in Ref. 55) that this is not a problem: The triaxiality parameter in the Nilsson potential, which was determined by the Nilsson Strutinsky calculation and used in the RPA calculation, is too small compared with the value estimated by the macroscopic rotor model. If the same value as that used in the particle-rotor model analysis is employed, the RPA calculation gives correct magnitudes of the $B(E2)$ ratio.[55]

In all the previous realistic calculations of the RPA wobbling excitations mentioned above, the Nilsson (modified oscillator) potential is used as a nuclear mean-field. The problem of the Nilsson potential applied to high-spin cranking calculations is well-known: The moment of inertia is overestimated due to the $\boldsymbol{l}^2$ potential, see e.g. Ref. 56). The simplest way to avoid this problem is to apply the Strutinsky renormalization to the angular momentum expectation value, which cannot be used in the RPA calculation. In fact the absolute value of the moment of inertia is about 30% overestimated in the previous calculations.[46)–48)] More fundamental remedy is to include a new field-coupling in order to restore the local Galilean invariance broken by the velocity dependent potential like the $\boldsymbol{l}^2$ term, which was suggested in Ref. 5) and formulated in Ref. 57). Based on this formalism the correction to the cranking term was incorporated in the high-spin cranking calculation in Ref. 58). Recently, this method has been successfully employed in Ref. 59), and the author of Ref. 59) claimed that the problem of the Nilsson potential is solved. However, when this method is applied, we found that no RPA solutions corresponding to the wobbling phonon were obtained for the TSD nuclei in the Lu and Hf region. The reason is clear: The method is only applied to one component along the cranking axis

among three possible rotational axes. The field-coupling to restore the local Galilean invariance is realized as a residual two-body interaction, which is composed of three components corresponding to the infinitesimal rotations about each Cartesian axis, in the original formulation.[57] The method to include the correction to the cranking model in Refs. 58) and 59) is derived by using the mean-field (HF or HFB) approximation to this residual interaction, so that only the component of the cranking (x-) axis is effective. All the three components, especially the perpendicular (y, z-) components, are necessary to be included for the description of the wobbling excitation, which is of generic three dimensional rotation. Thus, the whole additional residual interaction should be included in the RPA wobbling calculation.

The present work is along the same line as those works based on the formalism of the cranked mean-field and the RPA. However, we use the Woods-Saxon potential as a nuclear mean-field to avoid the problem mentioned above because there is no velocity dependent part of the potential (except for the spin-orbit term). Apart from the problem of the velocity dependence, the Woods-Saxon potential is believed to be more realistic than the Nilsson potential. It is desirable to confirm the existence of the wobbling-like RPA solutions also in this mean-field potential. Moreover, we show that the original formulation of Ref. 32) should be slightly modified for the general deformed mean-field like the Woods-Saxon potential, although the actual numerical difference is found to be small. The paper is organized as follows: The basic formulation of the wobbling RPA theory[32),42)] is reviewed and the necessary modification is explained in §2. The results of numerical calculations are presented in §3, where the detailed and systematic analyses are performed. Section 4 is devoted to a summary. A part of the present work was presented in a conference report.[60)]

§2. RPA wobbling theory

Although it may be desirable to perform the full selfconsistent cranked HFB plus RPA calculation by using a realistic two-body effective interaction, such as one of Skyrme forces or Gogny forces, it is still not very easy because all the symmetries except the parity and signature are broken in the triaxial superdeformed (TSD) rotational band. One way is to use a simple mean-field and a schematic interaction such as the pairing plus quadrupole interaction.[27)] We take a different approach: Starting from a reliable nuclear mean-field for triaxially deformed nuclei, we construct the residual interaction that is suitable to describe the nuclear wobbling motion. In this way, we can investigate the properties of the wobbling mode for any given mean-fields, e.g., its dependence on the triaxiality or the pairing gap. In this section, after explaining the Woods-Saxon potential and how to construct the residual interaction, we discuss the RPA wobbling formalism, which needs to be slightly modified from the original one by Marshalek.[32)]

2.1. *Triaxially deformed Woods-Saxon potential*

The triaxially deformed Woods-Saxon potential considered in this work is a

standard one widely used in the study of high-spin states:[61)–63)]

$$V_{\rm WS}(\boldsymbol{r}) = V_{\rm c}(\boldsymbol{r}) + \lambda_{\rm so}\left(\frac{\hbar}{2M_{\rm red}c}\right)^2 \left(\boldsymbol{\nabla} V_{\rm c}(\boldsymbol{r})\right)\cdot\left(\boldsymbol{\sigma}\times\frac{1}{i}\boldsymbol{\nabla}\right). \tag{2·1}$$

The first term is the central part and the second is the spin-orbit term. $M_{\rm red} = \frac{A-1}{A}M$ with A being the mass number and M being the nucleon mass, and $\boldsymbol{\sigma}$ is the Pauli matrices (the nucleon spin $\boldsymbol{s} = \frac{\hbar}{2}\boldsymbol{\sigma}$). The explicit form of the central potential is

$$V_{\rm c}(\boldsymbol{r}) = \frac{V}{1+\exp({\rm dist}_{\Sigma}(\boldsymbol{r})/a)}, \tag{2·2}$$

where the strength V is given by

$$V = -V_0\times\left(1\pm\kappa\frac{N-Z}{A}\right), \quad \begin{cases} +\text{proton} \\ -\text{neutron} \end{cases}, \tag{2·3}$$

with Z and N being the proton and neutron numbers, respectively, and ${\rm dist}_{\Sigma}(\boldsymbol{r})$ is the distance between a given point $\boldsymbol{r}$ and the nuclear surface Σ, with a minus sign if $\boldsymbol{r}$ is inside Σ. The nuclear surface Σ in this work is parametrized by three deformation parameters, (β_2,γ,β_4), and is defined by the usual radius to solid-angle relation, $r = R(\Omega)$;

$$R(\Omega) = R_0\, c_{\rm v}(\beta_2,\gamma,\beta_4)\left[1+\sum_{K=0,\pm2} a_{2K}Y_{2K}(\Omega)+\sum_{K=0,\pm2,\pm4} a_{4K}Y_{4K}(\Omega)\right], \tag{2·4}$$

where $c_{\rm v}(\beta_2,\gamma,\beta_4)$ is determined by the volume conserving condition, and the coefficients a are given by

$$\begin{cases} a_{20} = \beta_2\cos\gamma, \\ a_{22} = a_{2-2} = -\frac{1}{\sqrt{2}}\beta_2\sin\gamma, \end{cases} \qquad \begin{cases} a_{40} = \frac{1}{6}\beta_4(5\cos^2\gamma+1), \\ a_{42} = a_{4-2} = -\sqrt{\frac{5}{6}}\beta_4\cos\gamma\sin\gamma, \\ a_{44} = a_{4-4} = \sqrt{\frac{35}{72}}\beta_4\sin^2\gamma. \end{cases} \tag{2·5}$$

The Coulomb potential, which is calculated by assuming the uniform charge distribution inside the surface Σ given by the central potential,

$$V_{\rm Coul}(\boldsymbol{r}) = \frac{3(Z-1)e^2}{8\pi R_0^3}\iint_{\Sigma}\frac{(\boldsymbol{r}-\boldsymbol{r}')\cdot d\boldsymbol{S}'}{|\boldsymbol{r}-\boldsymbol{r}'|}, \tag{2·6}$$

is added to the proton potential.

Table I. The parameters of the Woods-Saxon potential used in this work.[64)] Other physical constants used are $e^2/\hbar c$=137.03602, $\hbar c = 197.32891$ MeV·fm, and $Mc^2 = 938.9059$ MeV. A in the table denotes the mass number of nucleus.

V_0 (MeV)	$\kappa_{\rm c}$	$\kappa_{\rm so}$	$R_{0\rm c}$ (fm)	$R_{0\rm so}$	a (fm)	$\lambda_{\rm so}$
53.7	0.63	0.25461	$1.193\,A^{1/3}+0.25$	$0.969\times R_{0\rm c}$	0.68	26.847

The potential is completely specified by the parameters, V_0, κ, R_0, a, and λ. In this work we use a set of those parameters provided by Ramon Wyss,[64] among which κ and R_0 are different in the central and spin-orbit potentials. These parameters are determined by the requirement that the moments of inertia and the quadrupole moments can be nicely reproduced systematically for medium and heavy nuclei throughout the nuclear chart. They are given in Table I.

It should be mentioned[55] that the triaxiality parameter γ in Eq. (2·5), for which we denote γ(pot:WS) if necessary, is considerably different from the one defined in terms of the quadrupole moments, γ(den). For example, $\gamma(\text{den}) = 20^\circ$ corresponds to $\gamma(\text{pot:WS}) \approx 30^\circ$ for the case of large deformation such as the TSD bands, which gives important consequences on the interpretation of the $B(E2)$ observed in the wobbling TSD bands (see Ref. 55)). This point will be discussed in more detail in §3.5.

2.2. *Residual interaction and RPA in the uniformly rotating (UR) frame*

The method to construct the residual interaction is discussed in relation to the wobbling motion in Ref. 65). The idea is based on the decoupling of the rotational Nambu-Goldstone (NG) modes, i.e., the angular momentum operators J_i $(i = x, y, z)$, within the RPA.[66] The same idea is formulated in the context of the particle-vibration coupling theory.[5] Although the following discussions are essentially the same as those of Refs. 32) and 33), we recapitulate them because some of their results are used in the later discussions in order to make clear the point that should be modified from the original RPA wobbling theory.[32] It should be noted that the signature, the π rotation about the cranking axis (x-axis), is a good quantum number, and only the part of the RPA equation which transfer the signature quantum number α by $\Delta\alpha = 1$, the so-called signature $(-)$-part, is relevant to the wobbling motion. Therefore, we consider only the corresponding part of the residual interaction.

Starting from the general mean-field hamiltonian, h, which, in the present work, is composed of the kinetic energy, the Woods-Saxon potential, the Coulomb potential, and the pairing part (see §3.1), the relevant part of the residual interaction is given by

$$H_{\text{res}} = -\frac{1}{2}\chi_y F_y^2 - \frac{1}{2}\chi_z (iF_z)^2, \tag{2·7}$$

where the operators F_y and F_z are defined by

$$F_y \equiv [h, iJ_y], \quad iF_z \equiv i[h, J_z]. \tag{2·8}$$

The strengths of the interaction are determined by the decoupling condition of the NG modes, J_y and J_z, for the total hamiltonian, $H \equiv h + H_{\text{res}}$,

$$[H, J_{y,z}]_{\text{RPA}} = [h + H_{\text{res}}, J_{y,z}]_{\text{RPA}} = 0, \tag{2·9}$$

where the subscript RPA means that the commutator is evaluated within the RPA order, leading to

$$1/\chi_y = \big\langle [[h, iJ_y], iJ_y] \big\rangle, \quad 1/\chi_z = -\big\langle [[h, J_z], J_z] \big\rangle. \tag{2·10}$$

Here (and hereafter if not stated explicitly) the expectation values are taken with respect to the cranked mean-field state (the generalized product state) $|\Phi(\omega_{\rm rot})\rangle$, which is a vacuum state of the quasiparticles in the uniformly rotating frame about the x-axis,

$$h - \omega_{\rm rot} J_x = \sum_\alpha E_\alpha a_\alpha^\dagger a_\alpha, \tag{2·11}$$

where $\omega_{\rm rot}$ is the rotational (cranking) frequency, E_α is the energy of the quasiparticle eigenstate $|\alpha\rangle$ in the rotating frame (quasiparticle routhian), and $a_\alpha^\dagger$ is its quasiparticle creation operator. It should be stressed that the vacuum mean-field state, $|\Phi(\omega_{\rm rot})\rangle$, determines the strengths in contrast to the conventional case, where the two-body interaction, such as the QQ force, is given and it determines the vacuum mean-field state. This is very important to guarantee the NG mode decoupling: It is usually a numerically demanding task to satisfy the selfconsistency between the interaction and the vacuum mean-field state in such a level as to exactly satisfy the NG mode decoupling.

The creation operator of the RPA eigenmode excited on the cranked vacuum state $|\Phi(\omega_{\rm rot})\rangle$, i.e., the one in the uniformly rotating (UR) frame, is given as a linear combination of the two-quasiparticle excited states,

$$X_n^\dagger = \sum_{\alpha<\beta} \left[\psi_n(\alpha\beta) a_\alpha^\dagger a_\beta^\dagger + \phi_n(\alpha\beta) a_\beta a_\alpha \right], \tag{2·12}$$

and is obtained by solving the RPA equation in the UR frame,

$$[H_{\rm UR}, X_n^\dagger]_{\rm RPA} = \omega_n X_n^\dagger, \quad H_{\rm UR} \equiv H - \omega_{\rm rot} J_x, \tag{2·13}$$

where ω_n is the corresponding RPA eigenfrequency. Here and hereafter we use $\hbar = 1$ unit for simplicity.

The operators which play a key role for defining the principal axis (PA) frame discussed in the next subsection, are the non-diagonal part of the (mass) quadrupole tensor operators. What is relevant to the RPA wobbling theory is their signature $(-)$ part,

$$Q_y \equiv Q_{21}^{(-)} = -\sqrt{\frac{15}{4\pi}} \sum_{a=1}^A (xz)_a, \quad Q_z \equiv Q_{22}^{(-)} = i\sqrt{\frac{15}{4\pi}} \sum_{a=1}^A (xy)_a, \tag{2·14}$$

where the z-axis is chosen as a quantization axis of the signature classified quadrupole tensor,

$$Q_{2K}^{(\pm)} = \frac{1}{\sqrt{2(1+\delta_{K0})}} \big(Q_{2K} \pm Q_{2-K} \big). \quad (K = 0, 1, 2) \tag{2·15}$$

They are important also because the out-of-band $E2$ transition probabilities are calculated by their RPA matrix elements. The part composed of the two quasiparticle excitations only contributes within the RPA order, and it is denoted with the superscript (A) in the following:

$$(Q_y)^{(A)} = \sum_{\alpha<\beta} q_y(\alpha\beta) \big(a_\alpha^\dagger a_\beta^\dagger + a_\beta a_\alpha \big), \quad (Q_z)^{(A)} = \sum_{\alpha<\beta} q_z(\alpha\beta) \big(a_\alpha^\dagger a_\beta^\dagger - a_\beta a_\alpha \big), \tag{2·16}$$

where we used the phase convention[67] that the two-quasiparticle matrix elements in this and the following Eq. (2·17) are all real, $q_{y,z}(\alpha\beta) = q^*_{y,z}(\alpha\beta)$, $j_{y,z}(\alpha\beta) = j^*_{y,z}(\alpha\beta)$. As it can be easily checked, the signature $(-)$ part of the angular momentum operators,

$$(iJ_y)^{(A)} = \sum_{\alpha<\beta} j_y(\alpha\beta)\big(a^\dagger_\alpha a^\dagger_\beta - a_\beta a_\alpha\big), \quad (J_z)^{(A)} = \sum_{\alpha<\beta} j_z(\alpha\beta)\big(a^\dagger_\alpha a^\dagger_\beta + a_\beta a_\alpha\big), \tag{2·17}$$

combines into the RPA eigenmode corresponding to the NG mode in Eq. (2·13),

$$X^\dagger_{n=\mathrm{NG}} = \frac{1}{\sqrt{2\langle J_x\rangle}}\left[(iJ_y)^{(A)} + (J_z)^{(A)}\right], \tag{2·18}$$

with the eigenfrequency $\omega_{n=\mathrm{NG}} = \omega_{\mathrm{rot}}$. Here the expectation value of the angular momentum along the cranking axis can be written as $\langle J_x\rangle = 2\sum_{\alpha<\beta} j_y(\alpha\beta)j_z(\alpha\beta)$. In the same way, for the operators $F_{y,z}$ in Eq. (2·8),

$$(F_y)^{(A)} = \sum_{\alpha<\beta} f_y(\alpha\beta)\big(a^\dagger_\alpha a^\dagger_\beta + a_\beta a_\alpha\big), \quad (F_z)^{(A)} = \sum_{\alpha<\beta} f_z(\alpha\beta)\big(a^\dagger_\alpha a^\dagger_\beta - a_\beta a_\alpha\big), \tag{2·19}$$

and by the definition their matrix elements are expressed as

$$f_y(\alpha\beta) = E_{\alpha\beta} j_y(\alpha\beta) - \omega_{\mathrm{rot}} j_z(\alpha\beta), \quad f_z(\alpha\beta) = E_{\alpha\beta} j_z(\alpha\beta) - \omega_{\mathrm{rot}} f_y(\alpha\beta), \tag{2·20}$$

with $E_{\alpha\beta} \equiv E_\alpha + E_\beta$, and the force strengths as

$$\chi_y^{-1} = 2\sum_{\alpha<\beta} E_{\alpha\beta}\, j_y^2(\alpha\beta) - \omega_{\mathrm{rot}}\langle J_x\rangle, \quad \chi_z^{-1} = 2\sum_{\alpha<\beta} E_{\alpha\beta}\, j_z^2(\alpha\beta) - \omega_{\mathrm{rot}}\langle J_x\rangle. \tag{2·21}$$

Since the residual interaction is of the multi-component separable type, it is straightforward to solve the RPA equation by means of the dispersion matrix technique.[44),45] The forward and backward amplitudes in Eq. (2·12) are given by

$$\begin{cases} \psi_n(\alpha\beta) = \dfrac{f_y(\alpha\beta)\chi_y\mathcal{F}_y(n) + f_z(\alpha\beta)\chi_z\mathcal{F}_z(n)}{E_{\alpha\beta} - \omega_n}, \\ \phi_n(\alpha\beta) = \dfrac{-f_y(\alpha\beta)\chi_y\mathcal{F}_y(n) + f_z(\alpha\beta)\chi_z\mathcal{F}_z(n)}{E_{\alpha\beta} + \omega_n}, \end{cases} \tag{2·22}$$

where the RPA transition matrix elements for the operator $F_{y,z}$ are defined by

$$\begin{aligned} \mathcal{F}_y(n) &\equiv \big\langle [X_n, F_y]\big\rangle = \sum_{\alpha<\beta}\big(\psi_n(\alpha\beta) - \phi_n(\alpha\beta)\big) f_y(\alpha\beta), \\ \mathcal{F}_z(n) &\equiv \big\langle [X_n, F_z]\big\rangle = \sum_{\alpha<\beta}\big(\psi_n(\alpha\beta) + \phi_n(\alpha\beta)\big) f_z(\alpha\beta), \end{aligned} \tag{2·23}$$

which are obtained by solving the following linear equation:

$$\begin{bmatrix} R_{yy}(\omega_n) - \chi_y^{-1}, & R_{yz}(\omega_n) \\ R_{zy}(\omega_n), & R_{zzs}(\omega_n) - \chi_z^{-1} \end{bmatrix} \begin{bmatrix} \chi_y\mathcal{F}_y(n) \\ \chi_z\mathcal{F}_z(n) \end{bmatrix} = 0. \tag{2·24}$$

Here the quantities in the matrix are given by

$$\begin{aligned} &R_{yy}(\omega) = D^{(1)}(f_y, f_y; \omega),\ R_{zz}(\omega) = D^{(1)}(f_z, f_z; \omega), \\ &R_{yz}(\omega) = R_{zy}(\omega) = D^{(2)}(f_y, f_z; \omega), \end{aligned} \tag{2·25}$$

where the response functions $D^{(1,2)}$ are defined by

$$D^{(1)}(f,g;\omega) \equiv \sum_{\alpha<\beta} \frac{2E_{\alpha\beta} f(\alpha\beta) g(\alpha\beta)}{E_{\alpha\beta}^2 - \omega^2}, \quad D^{(2)}(f,g;\omega) \equiv \sum_{\alpha<\beta} \frac{2\omega f(\alpha\beta) g(\alpha\beta)}{E_{\alpha\beta}^2 - \omega^2}. \tag{2·26}$$

Thus the RPA eigenfrequency $\omega = \omega_n$ is obtained by solving the dispersion equation

$$\det \left| \begin{array}{cc} R_{yy}(\omega) - \chi_y^{-1}, & R_{yz}(\omega) \\ R_{zy}(\omega), & R_{zz}(\omega) - \chi_z^{-1} \end{array} \right| = 0, \tag{2·27}$$

and the norm of the corresponding solution $(\chi_i \mathcal{F}_i(n),\ i = y, z)$ is determined by the normalization condition $\sum_{\alpha<\beta}\big(\psi_n^2(\alpha\beta) - \phi_n^2(\alpha\beta)\big) = 1$.

In the case of the residual interaction (2·7) with (2·8), the NG mode (2·18) can be explicitly separated out from the equation. By inserting Eqs. (2·20) and (2·21) into Eq. (2·24), the matrix in Eq. (2·24) can be written as

$$\left[\begin{array}{cc} \omega_n B_y(\omega_n) - \omega_{\rm rot} A_z(\omega_n), & \omega_n A_z(\omega_n) - \omega_{\rm rot} B_y(\omega_n) \\ \omega_n A_y(\omega_n) - \omega_{\rm rot} B_z(\omega_n), & \omega_n B_z(\omega_n) - \omega_{\rm rot} A_y(\omega_n) \end{array} \right], \tag{2·28}$$

with the definitions,

$$\left\{ \begin{array}{l} A_y(\omega) \equiv \omega_{\rm rot}\big(\mathcal{J}_x - \mathcal{J}_y(\omega)\big) + \omega \mathcal{J}_{yz}(\omega), \\ A_z(\omega) \equiv \omega_{\rm rot}\big(\mathcal{J}_x - \mathcal{J}_z(\omega)\big) + \omega \mathcal{J}_{yz}(\omega), \\ B_y(\omega) \equiv \omega \mathcal{J}_y(\omega) - \omega_{\rm rot} \mathcal{J}_{yz}(\omega), \\ B_z(\omega) \equiv \omega \mathcal{J}_z(\omega) - \omega_{\rm rot} \mathcal{J}_{yz}(\omega), \end{array} \right. \tag{2·29}$$

and

$$\begin{aligned} \mathcal{J}_x \equiv \frac{\langle J_x \rangle}{\omega_{\rm rot}}, \quad \mathcal{J}_y(\omega) \equiv D^{(1)}(j_y, j_y; \omega), \\ \mathcal{J}_z(\omega) \equiv D^{(1)}(j_z, j_z; \omega),\ \ \mathcal{J}_{yz}(\omega) \equiv D^{(2)}(j_y, j_z; \omega). \end{aligned} \tag{2·30}$$

Then Eq. (2·24) can be cast into the form

$$\left[\begin{array}{cc} \omega_{\rm rot} - \omega_n, & 0 \\ 0, & \omega_{\rm rot} + \omega_n \end{array} \right] \left[\begin{array}{cc} A_z(\omega_n) + B_y(\omega_n), & B_z(\omega_n) + A_y(\omega_n) \\ A_z(\omega_n) - B_y(\omega_n), & B_z(\omega_n) - A_y(\omega_n) \end{array} \right] \left[\begin{array}{c} \chi_y \mathcal{F}_y(n) \\ \chi_z \mathcal{F}_z(n) \end{array} \right] = 0, \tag{2·31}$$

from which the $\omega_{n=\rm NG} = \omega_{\rm rot}$ NG solution is apparent, because by using Eq. (2·18) the NG amplitudes $(\chi_i \mathcal{F}_i,\ i = y, z)$ reduce to

$$\left[\begin{array}{c} \chi_y \mathcal{F}_y(n = \rm NG) \\ \chi_z \mathcal{F}_z(n = \rm NG) \end{array} \right] = \frac{1}{\sqrt{2\langle J_x \rangle}} \left[\begin{array}{c} 1 \\ 1 \end{array} \right]. \tag{2·32}$$

Thus, the linear equation and the dispersion equation for the non-NG solutions, $\omega_n \neq \omega_{\rm rot}$, are

$$\left[\begin{array}{cc} B_y(\omega_n), & A_y(\omega_n) \\ A_z(\omega_n), & B_z(\omega_n) \end{array} \right] \left[\begin{array}{c} \chi_y \mathcal{F}_y(n) \\ \chi_z \mathcal{F}_z(n) \end{array} \right] = 0, \quad \det \left| \begin{array}{cc} B_y(\omega), & A_y(\omega) \\ A_z(\omega), & B_z(\omega) \end{array} \right| = 0, \tag{2·33}$$

which was first derived in Ref. 33). Alternatively, Eq. (2·24) can be cast into another form

$$\begin{bmatrix} A_y(\omega_n), B_z(\omega_n) \\ B_y(\omega_n), A_z(\omega_n) \end{bmatrix} \begin{bmatrix} \bar{\Omega}_y(n) \\ \bar{\Omega}_z(n) \end{bmatrix} = 0, \tag{2·34}$$

with the definitions,

$$\bar{\Omega}_y(n) \equiv \omega_n \chi_y \mathcal{F}_y(n) - \omega_{\rm rot}\chi_z \mathcal{F}_z(n), \quad \bar{\Omega}_z(n) \equiv \omega_n \chi_z \mathcal{F}_z(n) - \omega_{\rm rot}\chi_y \mathcal{F}_y(n). \tag{2·35}$$

Again, this equation contains the trivial NG solution (2·32), i.e., $\bar{\Omega}_y(n) = \bar{\Omega}_z(n) = 0$, with $\omega_{n=\rm NG} = \omega_{\rm rot}$. For the non-NG solutions, $\bar{\Omega}_y(n)/\bar{\Omega}_z(n) = -B_z(\omega_n)/A_y(\omega_n) = -A_z(\omega_n)/B_y(\omega_n)$, therefore, by defining

$$\bar{\mathcal{J}}_y^{\rm eff}(n) \equiv \mathcal{J}_y(\omega_n) - \mathcal{J}_{yz}(\omega_n)\frac{A_y(\omega_n)}{B_z(\omega_n)}, \quad \bar{\mathcal{J}}_z^{\rm eff}(n) \equiv \mathcal{J}_z(\omega_n) - \mathcal{J}_{yz}(\omega_n)\frac{A_z(\omega_n)}{B_y(\omega_n)}, \tag{2·36}$$

Eq. (2·34) can be further changed into

$$\begin{bmatrix} \omega_{\rm rot}\big(\mathcal{J}_x - \bar{\mathcal{J}}_y^{\rm eff}(n)\big), & \omega_n \bar{\mathcal{J}}_y^{\rm eff}(n) \\ \omega_n \bar{\mathcal{J}}_z^{\rm eff}(n), & \omega_{\rm rot}\big(\mathcal{J}_x - \bar{\mathcal{J}}_z^{\rm eff}(n)\big) \end{bmatrix} \begin{bmatrix} \bar{\Omega}_y(n) \\ \bar{\Omega}_z(n) \end{bmatrix} = 0, \tag{2·37}$$

from which the wobbling phonon energy is formally solved,

$$\omega_n = \omega_{\rm rot}\sqrt{\frac{\big(\mathcal{J}_x - \bar{\mathcal{J}}_y^{\rm eff}(n)\big)\big(\mathcal{J}_x - \bar{\mathcal{J}}_z^{\rm eff}(n)\big)}{\bar{\mathcal{J}}_y^{\rm eff}(n)\bar{\mathcal{J}}_z^{\rm eff}(n)}}. \tag{2·38}$$

This equation is equivalent to Eq. (2·33) and was first derived by Marshalek.[32)]

In the original formulation of Ref. 32), the quantities $\bar{\Omega}_{y,z}(n)$ and $\bar{\mathcal{J}}_{y,z}^{\rm eff}(n)$ are interpreted as the amplitudes of y, z-components of the angular frequency vector and of moments of inertia, respectively, in the principal axis (PA) frame, when the n-th RPA mode is excited. However, this is *not* the case for the general deformed mean-field like in the present work, which is the subject of the next subsection.

For the sake of completeness, the $E2$ and $M1$ transition probabilities from the n-th RPA phonon excited rotational band to the vacuum band are calculated, within the lowest order in the $1/I$ expansion consistent to the RPA order,[43)] by

$$B(E2; In \to I \pm 1{\rm vac}) \approx \big|\big\langle [Q^E_{2\pm1}, X^\dagger_n]\big\rangle\big|^2, \tag{2·39}$$

$$B(M1; In \to I \pm 1{\rm vac}) \approx \big|\big\langle [\mu_{1\pm1}, X^\dagger_n]\big\rangle\big|^2. \tag{2·40}$$

Here the electric $E2$ and $M1$ operators defined with respect to the x-axis, $Q^E_{2\nu}$ and $\mu_{1\nu}$ ($\nu = \pm1$) are given by

$$Q^E_{2\pm1} = \frac{i}{\sqrt{2}}\big(Q^{E(-)}_{21} \pm Q^{E(-)}_{22}\big) = \frac{i}{\sqrt{2}}\big(Q^E_y \pm Q^E_z\big), \tag{2·41}$$

$$\mu_{1\pm1} = \pm\frac{i}{\sqrt{2}}\big(i\mu_y \mp \mu_z\big), \tag{2·42}$$

where the electric quadrupole operators, $Q^{E(-)}_{2K}$ ($K = 1, 2$) and $Q^E_{y,z}$, are defined in the same way as in Eqs. (2·15) and (2·14), but only the proton contributions are

included and the electric charge e is multiplied. The magnetic moment operator μ_k $(k = x, y, z)$ is given as usual,

$$\mu_k = \sqrt{\frac{3}{4\pi}}\,\mu_N \sum_{a=1}^{A} \bigl(g_l^{(\tau)} l_k + g_s^{(\tau)} s_k\bigr)_a. \quad (\tau = \pi, \nu) \tag{2·43}$$

As for the in-band stretched $E2$ transition probabilities, those in the phonon excited band and the vacuum band are the same in the RPA order and are calculated by

$$B(E2; I \to I \pm 2) \approx \frac{1}{2}\bigl|\langle Q^E_{2\pm2}\rangle\bigr|^2 = \frac{1}{2}\Bigl|\Bigl\langle\Bigl(\frac{\sqrt{3}}{2}Q^{E(+)}_{20} + \frac{1}{2}Q^{E(+)}_{22}\Bigr)\Bigr\rangle\Bigr|^2. \tag{2·44}$$

2.3. *Interpretation of the RPA eigenmode in the principal axis (PA) frame*

All the calculations of the observable quantities such as excitation energies and electromagnetic transition probabilities can be done within the RPA in the UR frame as has been reviewed in the last subsection. It is, however, necessary to go into the PA frame in order to interpret the obtained RPA eigenmode and compare its property with that of the wobbling motion, which is introduced in the macroscopic rotor model. Furthermore, the transformation is inevitable to investigate how much the angular momentum vector, or the angular frequency vector, tilts or wobbles around the main rotation axis. This has been done by Marshalek,[32] and reviewed from a slightly general view point in Ref. 42) in the light of the quantum theory of collective coordinates.[29),31)] In this subsection, we recapitulate some results from Ref. 42), in order to show that a slight modification of the original formulation in 32) is necessary for the general deformed mean-field.

The transformation from the laboratory frame to the UR frame is an unitary transformation so that the RPA in the UR frame satisfies all the usual properties,[27)] e.g., the completeness relation. Therefore, the two-quasiparticle excitation part of the quadrupole operators in Eq. (2·16) can be expanded in terms of the RPA eigenmodes,

$$(Q_y)^{(A)} = \sum_{n:\mathrm{all}} \mathcal{Q}_y(n)\bigl(X_n^\dagger + X_n\bigr), \quad (Q_z)^{(A)} = \sum_{n:\mathrm{all}} \mathcal{Q}_z(n)\bigl(X_n^\dagger - X_n\bigr), \tag{2·45}$$

where the amplitudes $\mathcal{Q}_{y,z}(n)$ are calculated by

$$\begin{aligned}
\mathcal{Q}_y(n) &\equiv \bigl\langle[X_n, Q_y]\bigr\rangle = \sum_{\alpha<\beta}\bigl(\psi_n(\alpha\beta) - \phi_n(\alpha\beta)\bigr)q_y(\alpha\beta), \\
\mathcal{Q}_z(n) &\equiv \bigl\langle[X_n, Q_z]\bigr\rangle = \sum_{\alpha<\beta}\bigl(\psi_n(\alpha\beta) + \phi_n(\alpha\beta)\bigr)q_z(\alpha\beta).
\end{aligned} \tag{2·46}$$

In particular, the NG mode contribution is contained in Eq. (2·45),

$$\mathcal{Q}_y(n = \mathrm{NG}) = -\frac{2\alpha_y R^2}{\sqrt{2\langle J_x\rangle}}, \quad \mathcal{Q}_z(n = \mathrm{NG}) = \frac{2\alpha_z R^2}{\sqrt{2\langle J_x\rangle}}, \tag{2·47}$$

where $R^2 \equiv \langle \sum_{a=1}^{A} (\boldsymbol{r}^2)_a \rangle$ is the mean square radius and $\alpha_y(\alpha_z)$ describes the deformation around the $y\,(z)$-axis,

$$2\alpha_y R^2 \equiv \sqrt{\frac{15}{4\pi}} \Big\langle \sum_{a=1}^{A} (x^2 - z^2)_a \Big\rangle = \big\langle [iJ_y, Q_y] \big\rangle = 2 \sum_{\alpha<\beta} j_y(\alpha\beta) q_y(\alpha\beta),$$

$$2\alpha_z R^2 \equiv \sqrt{\frac{15}{4\pi}} \Big\langle \sum_{a=1}^{A} (x^2 - y^2)_a \Big\rangle = \big\langle [J_z, Q_z] \big\rangle = 2 \sum_{\alpha<\beta} j_z(\alpha\beta) q_z(\alpha\beta). \tag{2·48}$$

In contrast, the two-quasiparticle excitation part of the angular momentum operators are composed purely of the NG mode,

$$(iJ_y)^{(A)} = \sqrt{\frac{\langle J_x \rangle}{2}} \big(X^\dagger_{\rm NG} - X_{\rm NG} \big), \quad (J_z)^{(A)} = \sqrt{\frac{\langle J_x \rangle}{2}} \big(X^\dagger_{\rm NG} + X_{\rm NG} \big). \tag{2·49}$$

Now let us consider the behavior of the angular momentum vector and the angular frequency vector when the RPA wobbling mode is excited, from which the moments of inertia are naturally introduced. We do not go into the full details of the theory, but briefly mention the procedure. As it is well-known, the (three dimensional) cranking prescription can be viewed as a result of the constraints, $J_i = I_i$ $(i = x, y, z)$, where I_i are time-dependent constants in the semiclassical theory,[35),38)] or are the total angular momentum operators in the rotor model (i.e., the differential operators with respect to the Euler angles) in the quantum theory of collective coordinates.[30)] This kind of constraints is called the first class constraints in the general theory,[68)] and one has to impose the second class constraints, i.e., the PA frame condition in this case, in order to develop the consistent framework of the quantum[29)] or the classical canonical[40)] theory. The second class constraints can be, in principle, arbitrarily chosen (the gauge condition), and the physical observables should not depend on the choice. However, the actual choice is important for the physical picture; recall, e.g., the choice of the center of mass coordinate in the case of the translational motion. Here we take the following PA frame condition;[28),32),35)] the non-diagonal part of the quadrupole tensor should vanish identically:

$$(Q_y)_{\rm PA} \equiv 0, \quad (Q_z)_{\rm PA} \equiv 0, \tag{2·50}$$

(the constraint for the x-component, i.e., $(Q_x)_{\rm PA} \equiv (Q^{(+)}_{21})_{\rm PA} \equiv 0$, is automatically satisfied in the RPA order), where the subscript PA denotes that the quantity is expressed in the PA frame.

This condition relates the collective coordinates, i.e., the Euler angles in the present case, to the nucleon degrees of freedom. Although it is a difficult task to obtain the relation in general, it has been shown in Ref. 32) that this relation can be solved within the small amplitude limit (RPA). The UR frame is transformed to the PA frame by the rotation in terms of the dynamical Euler angle variables Θ,

$$(\mathcal{O})_{\rm PA} = U(\Theta) \mathcal{O} U^{-1}(\Theta), \tag{2·51}$$

for an arbitrary operator $\mathcal{O}$. Here we omit the subscript UR for the quantity in the UR frame. Within the RPA order,[32)]

$$U(\Theta) \approx 1 - i\theta \big(\sin\psi J_y + \cos\psi J_z \big), \tag{2·52}$$

where $\Theta = (\psi, \theta, \phi)$ are Euler angles with respect to the x-axis (see Ref. 32)), and the small amplitude limit, $\theta \ll 1$, is used. From Eqs. (2·52) and (2·51),

$$(\mathcal{O})_{\rm PA} \approx \mathcal{O} + \theta \sin\psi \big\langle [\mathcal{O}, iJ_y] \big\rangle + i\theta \cos\psi \big\langle [\mathcal{O}, J_z] \big\rangle, \tag{2·53}$$

and applying this to Eq. (2·50), one obtains

$$\theta \sin\psi = \frac{Q_y}{2\alpha_y R^2}, \quad i\theta\cos\psi = \frac{Q_z}{2\alpha_z R^2}. \tag{2·54}$$

In this way the collective Euler-angle variables can be expressed directly by the nucleon degrees of freedom within the RPA order, i.e., the constraint conditions are approximately solved (the remaining angle ϕ does not play any role within the RPA order). Applying the transformation (2·53) to the angular momentum operators,

$$\begin{aligned}
(iJ_y)^{(A)}_{\rm PA} &= \Big(iJ_y - \frac{\langle J_x\rangle}{2\alpha_z R^2} Q_z\Big)^{(A)} = -\langle J_x\rangle \sum_{n\neq {\rm NG}} r_z(n)\big(X^\dagger_n - X_n\big), \\
(J_z)^{(A)}_{\rm PA} &= \Big(J_z + \frac{\langle J_x\rangle}{2\alpha_y R^2} Q_y\Big)^{(A)} = \langle J_x\rangle \sum_{n\neq {\rm NG}} r_y(n)\big(X^\dagger_n + X_n\big),
\end{aligned} \tag{2·55}$$

namely, their amplitudes associated with the n-th RPA eigenmode in the PA frame are

$$\begin{aligned}
(J_y)_{\rm PA}(n) &\equiv \big\langle [X_n, (iJ_y)_{\rm PA}] \big\rangle = -\langle J_x\rangle\, r_z(n), \\
(J_z)_{\rm PA}(n) &\equiv \big\langle [X_n, (J_z)_{\rm PA}] \big\rangle = \langle J_x\rangle\, r_y(n),
\end{aligned} \tag{2·56}$$

with the definitions,

$$r_y(n) \equiv \frac{\mathcal{Q}_y(n)}{2\alpha_y R^2}, \quad r_z(n) \equiv \frac{\mathcal{Q}_z(n)}{2\alpha_z R^2}, \tag{2·57}$$

which describe the shape fluctuations (ratios of the dynamic fluctuations amplitude to the static deformations). Thus, the contribution of the NG mode, which will be identified as the collective coordinate, is driven out and only the intrinsic degrees of freedom remain in the PA frame. From Eq. (2·55) it is clear that the angular momentum vector fluctuates or wobbles about the main rotation axis (x-axis), when the n-th RPA phonon is excited. The quantity $r_{y,z}(n)$ represent their fluctuations;

$$r_y(n) = \frac{(J_z)_{\rm PA}(n)}{\langle J_x\rangle}, \quad r_z(n) = -\frac{(J_y)_{\rm PA}(n)}{\langle J_x\rangle}. \tag{2·58}$$

Therefore these quantities should be small $r_{y,z}(n) \ll 1$ in order for the RPA to be valid. Note that all the amplitudes $\mathcal{Q}_{y,z}(n)$ and $r_{y,z}(n)$ are real because of the present phase convention.

The angular frequency vector operators ($\Omega_i, i = x, y, z$) in the PA frame are introduced as Lagrange multipliers of the first class constraints, $J_i = I_i$, (i.e. the constraint term is $-\sum_i \Omega_i\,(J_i - I_i)$), and the dynamical time dependence of nucleon operators in the PA frame is generated by the hamiltonian in the PA frame,

$$H_{\rm PA} = H - \sum_i \Omega_i J_i \approx H_{\rm UR} - \Omega_y (J_y)_{\rm PA} - \Omega_z (J_z)_{\rm PA}, \tag{2·59}$$

within the RPA order, because $\Omega_x \approx \omega_{\rm rot}$. According to the general theory with constraints,[68] the angular frequency variables ($\Omega_{y,z}$) are determined by the consistency condition of the PA frame (gauge) condition, i.e., Eq. (2·50) should hold in arbitrary time,[32]

$$i\frac{d}{dt}(Q_{y,z})_{\rm PA} = \big([Q_{y,z}, H_{\rm PA}]\big)_{\rm PA} = 0. \tag{2·60}$$

Here $\big([Q_y, H_{\rm PA}]\big)_{\rm PA} \approx \big([Q_y, H_{\rm UR}]\big)_{\rm PA} + i\Omega_y\big\langle[Q_y, iJ_y]\big\rangle$, $\big([Q_z, H_{\rm PA}]\big)_{\rm PA} \approx \big([Q_z, H_{\rm UR}]\big)_{\rm PA} - \Omega_z\big\langle[Q_z, J_z]\big\rangle$, and $H_{\rm UR} \approx \sum_{n:{\rm all}} \omega_n(X_n^\dagger X_n + \frac{1}{2})$ within the RPA order, and using the transformation (2·53) for $\big([Q_{y,z}, H_{\rm UR}]\big)_{\rm PA}$, we obtain

$$\begin{aligned}(i\Omega_y)^{(A)} &= -\sum_{n\neq{\rm NG}} \big(\omega_n r_y(n) + \omega_{\rm rot} r_z(n)\big)\big(X_n^\dagger - X_n\big),\\ (\Omega_z)^{(A)} &= \sum_{n\neq{\rm NG}} \big(\omega_n r_z(n) + \omega_{\rm rot} r_y(n)\big)\big(X_n^\dagger + X_n\big),\end{aligned} \tag{2·61}$$

i.e., their amplitudes associated with the n-th RPA eigenmode are

$$\begin{aligned}\Omega_y(n) &\equiv \big\langle[X_n, i\Omega_y]\big\rangle = -\big(\omega_n r_y(n) + \omega_{\rm rot} r_z(n)\big),\\ \Omega_z(n) &\equiv \big\langle[X_n, \Omega_z]\big\rangle = \omega_n r_z(n) + \omega_{\rm rot} r_y(n).\end{aligned} \tag{2·62}$$

Again, the NG mode contribution cancels out completely. From Eq. (2·61) the angular frequency vector also fluctuates about the main rotation axis, and the moments of inertia in the PA frame are naturally introduced;

$$\begin{aligned}\mathcal{J}_y^{\rm eff}(n) &\equiv \frac{(J_y)_{\rm PA}(n)}{\Omega_y(n)} = \frac{\mathcal{J}_x\omega_{\rm rot} r_z(n)}{\omega_n r_y(n) + \omega_{\rm rot} r_z(n)},\\ \mathcal{J}_z^{\rm eff}(n) &\equiv \frac{(J_z)_{\rm PA}(n)}{\Omega_z(n)} = \frac{\mathcal{J}_x\omega_{\rm rot} r_y(n)}{\omega_n r_z(n) + \omega_{\rm rot} r_y(n)}.\end{aligned} \tag{2·63}$$

It is clear that the moments of inertia thus defined are intimately connected to the PA frame condition (2·50) and determined by the RPA transition amplitudes of the $Q_{y,z}$ operators in Eq. (2·46).

From Eq. (2·63) the RPA eigenenergy and the $r_{y,z}(n)$ amplitudes can be represented in terms of these moments of inertia;[32),42)]

$$\omega_n = \omega_{\rm rot}\sqrt{\frac{\big(\mathcal{J}_x - \mathcal{J}_y^{\rm eff}(n)\big)\big(\mathcal{J}_x - \mathcal{J}_z^{\rm eff}(n)\big)}{\mathcal{J}_y^{\rm eff}(n)\mathcal{J}_z^{\rm eff}(n)}}, \tag{2·64}$$

i.e., the well-known formula in the rotor model[5] is recovered, and

$$r_y(n) = \frac{c_n}{\sqrt{2\langle J_x\rangle}}\left[\frac{1/\mathcal{J}_y^{\rm eff}(n) - 1/\mathcal{J}_x}{1/\mathcal{J}_z^{\rm eff}(n) - 1/\mathcal{J}_x}\right]^{1/4},\ r_z(n) = \frac{\sigma_n c_n}{\sqrt{2\langle J_x\rangle}}\left[\frac{1/\mathcal{J}_z^{\rm eff}(n) - 1/\mathcal{J}_x}{1/\mathcal{J}_y^{\rm eff}(n) - 1/\mathcal{J}_x}\right]^{1/4}, \tag{2·65}$$

where the quantity c_n and the sign σ_n are defined by

$$c_n = [\text{sign of } r_y(n)]\sqrt{2\langle J_x\rangle|r_y(n)r_z(n)|},\quad \sigma_n = \text{sign of } \big(r_y(n)r_z(n)\big). \tag{2·66}$$

Combining Eqs. (2·65), (2·57) and (2·39) with $Q^E_{2\nu}$ being replaced to $(eZ/A)Q_{2\nu}$, the rotor model expression for the out-of-band $B(E2)$ is also recovered, if $\sigma_n = +$ and $c_n^2 = 1$ are satisfied for the excitation of the n-th RPA eigenmode. This was first shown in Ref. 42), and the condition, $\sigma_n c_n^2 = 2\langle J_x\rangle\, r_y(n) r_z(n) = +1$, is used to identify the wobbling mode in a recent publication:[51] Note that $\sigma_n = -$ and $c_n = -1$ for the NG mode.

It must be emphasized that the discussion above is general and does not depend on specific choices either of residual interactions or of nuclear mean-fields. In the original formulation of Marshalek,[32] the arbitrary spherical mean-field and the QQ (plus the monopole pairing) force are assumed. It can be easily checked that the formulation is still valid for the selfconsistent anisotropic harmonic oscillator potential model,[5] for which the induced residual interaction is the doubly-stretched $Q''Q''$ force.[69)–72)] In such cases, the deformation is purely of quadrupole type, and the selfconsistent mean-field h leads for $F_{y,z}$ in Eq. (2·8) to

$$\chi_y F_y = -\frac{1}{2\alpha_y R^2}\, Q_y, \quad \chi_z F_z = \frac{1}{2\alpha_z R^2}\, Q_z, \tag{2·67}$$

and the two quantities $\bar{\Omega}_{y,z}(n)$ and $\bar{\mathcal{J}}^{\rm eff}_{y,z}(n)$ introduced in Eqs. (2·35) and (2·36) coincide with $\Omega_{y,z}(n)$ and $\mathcal{J}^{\rm eff}_{y,z}(n)$ in Eqs. (2·62) and (2·63), respectively. However, both are different generally, and the moments of inertia should not be calculated by Eq. (2·36) but by Eq. (2·63) for the general mean-field: This is exactly the point that the original formulation of Marshalek should be modified. Note that the two expressions of the RPA eigenenergy, Eqs. (2·38) and (2·64), give the same energy in spite of their appearance, because the eigenenergy is a gauge invariant quantity. As is discussed above, the moments of inertia are determined by the PA frame condition. Therefore, a possible alternative choice of the PA frame condition is $(F_{y,z})_{\rm PA} \equiv 0$ in place of $(Q_{y,z})_{\rm PA} \equiv 0$. Then the original theory is recovered, but now the rotor model expression for the out-of-band $B(E2)$ cannot be derived, because the operators $F_{y,z}$ are not strictly related to the quadrupole operators $Q_{y,z}$ for the general mean-field. We use Eq. (2·50) as the PA frame condition for the realistic calculations presented in §3.

2.4. *Remarks on the NG mode decoupling*

In the realistic calculations, it is not an easy task to exactly realize the NG mode decoupling, even though the microscopic hamiltonian satisfies the decoupling condition (2·9). For example, one has to use a truncation of the model space for diagonalization or a finite mesh size to solve differential equations of the single-particle states, which inevitably breaks the condition. When starting from some effective two-body force and the mean-field is determined by the HF (or HFB) procedure, a very accurate achievement of the selfconsistency between the interaction and the resultant mean-field is required. Practically, it often happens that even the decoupling condition (2·9) does not rigorously meet. For example, if one takes the Nilsson potential and the QQ force (or the doubly-stretched $Q''Q''$ force) as the total hamiltonian, then the rotational NG modes do not decouple exactly, because the general Nilsson potential[26] contains the "hexadecapole" deformed potential (the ϵ_4 defor-

mation), whose effects cannot be dealt with the simple QQ (or $Q''Q''$) force. Even if the ϵ_4 deformation is neglected, the $\boldsymbol{l}\cdot\boldsymbol{s}$ and $\boldsymbol{l}^2$ terms are those defined in the stretched coordinate in the standard Nilsson potential, so that they are not strictly spherically invariant.

The previous calculations of the TSD wobbling excitations in Refs. 46)–48) suffer from this problem; even though the ϵ_4 deformation was neglected in them, the stretched $\boldsymbol{l}\cdot\boldsymbol{s}$ and $\boldsymbol{l}^2$ terms are used. Then $\bar{\mathcal{J}}^{\rm eff}_{y,z}(n)$ in Eq. (2·36) does not coincide with $\mathcal{J}^{\rm eff}_{y,z}(n)$ in Eq. (2·63) rigorously. However, we have checked that the effect of the model space truncation is much severe, and the effect of the stretched $\boldsymbol{l}\cdot\boldsymbol{s}$ and $\boldsymbol{l}^2$ terms is very small; $\bar{\mathcal{J}}^{\rm eff}_{y,z}(n)$ and $\mathcal{J}^{\rm eff}_{y,z}(n)$ agree within 1% if enough numbers of the oscillator shells are included. In the recent calculations in Refs. 51) and 59), the non-stretched $\boldsymbol{l}\cdot\boldsymbol{s}$ and $\boldsymbol{l}^2$ terms are used in the Nilsson potential without the ϵ_4 deformation consistently, but the additional correction term, which recovers the Galilean invariance broken by the velocity dependent part, breaks the spherical symmetry. Therefore, in all these calculations, even if $\epsilon_4 = 0$, the NG mode decoupling was not strictly realized. In Refs. 51) and 59), one of the strengths of the $Q''Q''$ force is adjusted so that the RPA spectra contain the eigenenergy $\omega_n = \omega_{\rm rot}$, but then the corresponding eigenmode solution might not generally be the correct NG mode, Eq. (2·18), although it is claimed that such effect is small.[51),59)]

If the monopole (or seniority) pairing correlation is included in the mean-field, it can be an another source that disturbs the actual NG mode decoupling. Since the monopole (or seniority) pairing interaction gives divergent results in the full model space, some truncation scheme is necessary. Usually the energy truncation of the single-particle states is used, in which not all of the magnetic substates (m) for the orbital with a given angular momentum (j) are included in the pairing model space, and then the rotational invariance is broken. We have checked that this effect is very small if the pairing model space is not too small.

The method to construct the residual interaction that restores the rotational symmetry in §2.2 can be used to remedy (or avoid) this problem generally. Since the wobbling motion is intimately related to the rotational NG mode, we believe that it is important to respect its decoupling, and the method in §2.2 is a simple and flexible way to realize it.

§3. Results of numerical calculations

The purpose of the present work is to study the wobbling excitations of the triaxial superdeformed (TSD) bands in the Lu and Hf region. We first discuss the result of the mean-field calculations based on the new parameterization of the Woods-Saxon potential explained in §2.1, and then the result of the microscopic RPA calculations.

3.1. *Mean-field calculations*

Our mean-field hamiltonian is

$$h_\tau = t_\tau + V_{{\rm WS}\tau}(\boldsymbol{r}) + \delta_{\tau\pi}V_{\rm Coul}(\boldsymbol{r}) - \Delta_\tau(P^\dagger_\tau + P_\tau) - \lambda_\tau N_\tau, \tag{3·1}$$

Table II. The Strutinsky smoothed cranking moment of inertia in unit of $\hbar^2$/MeV for various nuclei and deformations. The corresponding rigid-body values are also included. The deformation parameters $(\beta_2, \gamma, \beta_4)$ are those used in Eq. (2·5).

nucleus	β_2	γ	β_4	$\widetilde{\mathcal{J}}_x$(WS)	$\widetilde{\mathcal{J}}_x$(Nils)	$\mathcal{J}_x$(rigid)
^{164}Er	0.258	0°	0.004	82.2	96.6	77.4
^{174}Hf	0.288	0°	−0.027	92.0	108.1	86.9
^{152}Dy	0.665	0°	0.134	97.1	112.6	90.6
^{163}Lu	0.420	18°	0.020	90.9	109.0	85.7

where $\tau = \pi, \nu$ distinguish the proton or neutron part, t is the kinetic energy term, $V_{\mathrm{WS}\tau}(\boldsymbol{r})$ is the Woods-Saxon potential in Eq. (2·1), $V_{\mathrm{Coul}}(\boldsymbol{r})$ is the Coulomb potential in Eq. (2·6), $P^\dagger$ and Δ are the monopole pair transfer operator and pairing gap, and N and λ are the number operator and the chemical potential, respectively. We have developed our own code, based on the program of Ref. 73), for the cranked Woods-Saxon calculation with pairing correlations included. The diagonalization is performed in two steps; first the Woods-Saxon (and Coulomb) potential ($\Delta = 0$ and $\omega_{\mathrm{rot}} = 0$) is diagonalized in the anisotropic harmonic oscillator basis, and then the cranked pairing problem (the HFB equation) is solved in the Woods-Saxon basis obtained in the first step.

The matrix elements of the Woods-Saxon (and Coulomb) potential with respect to the anisotropic oscillator basis are specified by the oscillator quantum numbers, (n_x, n_y, n_z). They are evaluated by using the recurrence relations of the Hermite polynomials[73] starting from the diagonal and subdiagonal matrix elements, which are calculated by the Gauss-Hermite quadrature formula. The three oscillator frequencies, $(\omega_x, \omega_y, \omega_z)$, are chosen to be inversely proportional to the mean radii of the x, y, z-directions, which are calculated geometrically by using the uniform density distribution based on the shape specified in Eq. (2·4) for given deformation parameters $(\beta_2, \gamma, \beta_4)$. The magnitude of the frequencies, $(\omega_x\omega_y\omega_z)^{1/3}$, is chosen to be $1.25 \times \omega_0$, with $\hbar\omega_0 = 41/A^{1/3}$ MeV. We use the truncation of the oscillator shells, $N_{\max} \equiv (n_x + n_y + n_z)_{\max} = 12$, in most of the calculations presented in this work. As for the Coulomb potential (2·6), it is evaluated by the Gauss-Legendre numerical integration if $\min_\Omega R(\Omega) < r < \max_\Omega R(\Omega)$, and by using the multipole expansion of $|\boldsymbol{r}-\boldsymbol{r}'|^{-1}$ up to $l_{\max} = 16$ if otherwise. Since we use the monopole pairing interaction, the truncation of the pairing model space is necessary. Woods-Saxon single-particle orbitals whose energy ϵ_i satisfies $|\epsilon_i - \lambda| \leq \hbar\omega_0$ are included in the pairing model space.

The main reason why we use the Woods-Saxon potential rather than the Nilsson potential is that the cranking moment of inertia $\mathcal{J}_x$ in Eq. (2·30) is overestimated unless the Strutinsky renormalization[26] is not performed for the expectation value $\langle J_x \rangle$. In order to show how this overestimation is greatly improved, we compare the cranking moment of inertia calculated by using the Woods-Saxon and the Nilsson potentials in Table II. The cranking moment of inertia is sensitive to the shell structure and the pairing correlation, so that we tabulated the Strutinsky smoothed moment of inertia, i.e., $\widetilde{\mathcal{J}}_x \equiv \widetilde{\langle J_x \rangle}/\omega_{\mathrm{rot}}$, without pairing for selected nuclei and

deformations in the rare earth region. This inertia $\widetilde{\mathcal{J}}_x$ is $\omega_{\rm rot}$-dependent but its dependence is known to be weak[56] (we have checked that the variations are less than 2% in the present examples), so that those at $\omega_{\rm rot} = 0.6$ MeV/$\hbar$ are tabulated. We also include the corresponding rigid-body values calculated by assuming the uniform density distribution with the radius $1.2 \times A^{1/3}$ fm. For the calculations of this $\widetilde{\mathcal{J}}_x$ and of the selfconsistent deformation of the TSD minima discussed in the followings, we employ the cranked Nilsson Strutinsky calculation of Ref. 74), where the $\Delta N_{\rm osc} = \pm 2$ coupling arising from the cranking term is included in an approximate way. The parameters of the present Woods-Saxon potential are given in Table I, and those of the Nilsson potential are taken from Ref. 75). The parametrizations of shape in the two potentials are different. We convert those of the Nilsson potential $(\epsilon_2, \gamma, \epsilon_4)$[75] to those of the Woods-Saxon potential $(\beta_2, \gamma, \beta_4)$ by requiring the same mean square radii of the x, y, z-directions, which are calculated geometrically by the uniform density distribution. We use this conversion between $(\beta_2, \gamma, \beta_4)$ and $(\epsilon_2, \gamma, \epsilon_4)$ throughout this work. As it is clear in Table II, the overestimation with the Nilsson potential by 25−27% is much more reduced to 6−7%; the remaining deviations are mainly due to the spin-orbit potential.

The result of Table II indicates that the single-particle orbitals of the present Woods-Saxon potential have correct radial size corresponding to $1.2 \times A^{1/3}$ fm, which is also apparent from the values of the radius parameters in Table I. In fact we have checked the proton and neutron density distributions calculated by using the present Woods-Saxon potential are quite similar to those obtained by the Hartree-Fock calculations using the standard Skyrme and Gogny forces.

In order to study the wobbling excitations of the TSD bands in the Lu and Hf region, we have to choose suitable deformation of the mean-field. The standard way is to search the minima in the Strutinsky method, but we are not yet able to perform reliable cranked Woods-Saxon Strutinsky calculations of the potential energy surface with fixed spin values. The main purpose of the present work is to confirm the existence of the wobbling excitation modes in the microscopic Woods-Saxon RPA calculation. Therefore, we rely on the results of the cranked Nilsson Strutinsky calculations for choosing the deformation parameters. The obtained deformation parameters for the yrast TSD band of ^{163}Lu, i.e., the band with the parity and signature $(\pi, \alpha) = (+, 1/2)$, change very little as functions of spin; they are about $\epsilon_2 = 0.41 - 0.38$, $\gamma = 19^\circ - 21^\circ$, and $\epsilon_4 = 0.03 - 0.05$ in the spin range $I^\pi = 25/2^+ - 97/2^+$. Taking the $(\epsilon_2, \gamma, \epsilon_4) = (0.39, 20^\circ, 0.04)$ as typical ones, the converted values are $(\beta_2, \gamma, \beta_4) = (0.42, 18^\circ, 0.02)$. We choose these values as reference values in the following calculations.

Now we discuss the single-particle properties of the present Woods-Saxon potential. In Fig. 1 the dependences of the proton and neutron single-particle energies on the deformation parameters $\beta_2(\beta_4)$ and γ are shown. It is clearly seen in the present Woods-Saxon potential that sizable shell gaps at $Z = 70 \sim 74$ for protons and $N = 92 \sim 96$ for neutrons are existing at the triaxial deformation $\gamma \approx 20^\circ$. When cranked, these shell gaps are responsible for the TSD bands systematically observed in nuclei in the Lu and Hf region.[13] Because of the relatively large deformation, $\beta_2 > 0.4$, the $N_{\rm osc} = 6$ proton orbitals resulting from the $\pi i_{13/2}$ state come

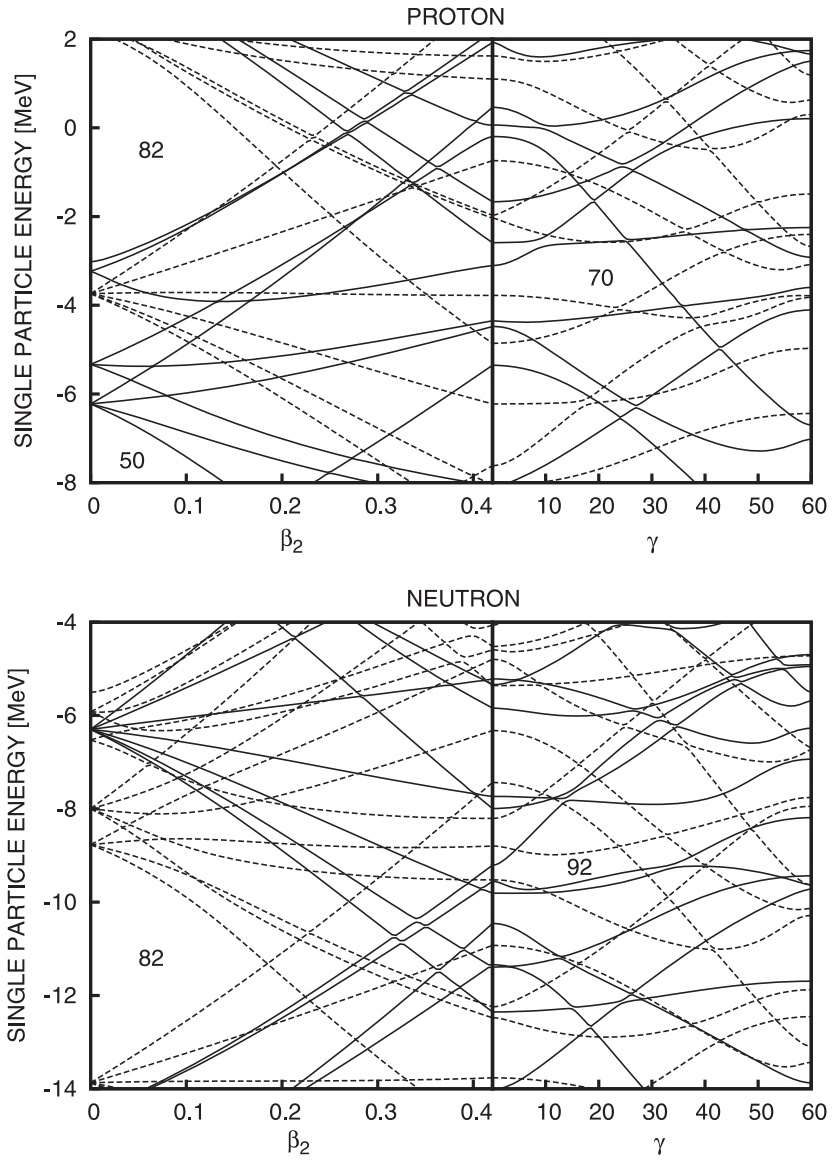

Fig. 1. The single-particle energies as functions of $\beta_2(\beta_4)$ and γ. The upper panel is for the proton energies and the lower panel for the neutron energies. In each figure the left part is drawn by changing β_2 (β_4) from 0 to 0.42 (from 0 to 0.02) with keeping $\gamma = 0$, while the right part by changing γ from 0° to 60° with keeping $(\beta_2, \beta_4) = (0.42, 0.02)$. The solid (dashed) lines are used for positive (negative) parity orbitals.

down near to the Fermi energy of the $Z \approx 71$ system, the lowest state of which is occupied in the yrast TSD band in Lu nuclei. It is well-known that the occupation of this down-sloping and highly-alignable orbitals increases the deformation from the normal deformed, $\beta_2 \approx 0.2$ and $\gamma \approx 0^\circ$, to the triaxially superdeformed shape, $\beta_2 \approx 0.4$ and $\gamma \approx 20^\circ$.

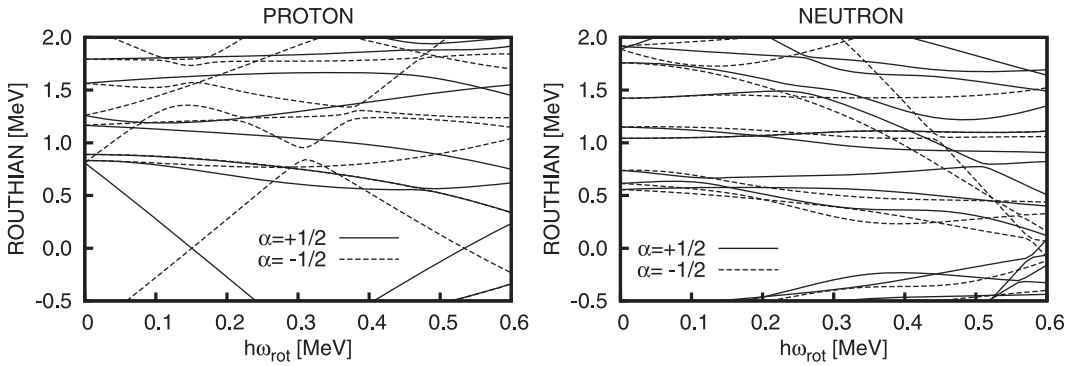

Fig. 2. The quasiparticle routhians as functions of the rotational frequency suitable for ^{163}Lu. The fixed deformation parameters $(\beta_2, \gamma, \beta_4) = (0.42, 18^\circ, 0.02)$ and the fixed pairing gaps $\Delta_\pi = \Delta_\nu = 0.5$ MeV are used. The left panel is for the quasiproton energies and the right panel for the quasineutron energies. The solid (dashed) lines are used for signature $\alpha = 1/2$ ($\alpha = -1/2$) orbitals.

The proton and neutron pairing gaps, Δ_π and Δ_ν, respectively, are also important mean-field parameters, for which we know very little in the TSD bands. Therefore, we use constant values for qualitative investigation of the TSD bands and of the wobbling excitations on them. We will discuss the result where the pairing gaps are changed in §3.4. The chemical potentials λ_π and λ_ν are always adjusted to reproduce the correct proton and neutron numbers, $\langle N_\pi \rangle = Z$ and $\langle N_\nu \rangle = N$. We show the quasiparticle energies (routhians) obtained by diagonalizing the cranked mean-field hamiltonian, Eq. (2·11), in Fig. 2, as functions of the rotational frequency. Constant pairing gaps, $\Delta_\pi = \Delta_\nu = 0.5$ MeV, are used with the reference deformation, $(\beta_2, \gamma, \beta_4) = (0.42, 18^\circ, 0.02)$ suitable for ^{163}Lu. It is clear that there is no crossing of the neutron quasiparticle before $\omega_{\rm rot} \approx 0.6$ MeV/$\hbar$. In contrast, one highly-alignable $\alpha = 1/2$ proton quasiparticle is clearly seen; its main component is the $N_{\rm osc} = 6$ oscillator shell coming down from the $\pi i_{13/2}$ orbitals. This $N_{\rm osc} = 6$ quasiproton is always occupied in the lowest TSD configuration of ^{163}Lu and contributes to the alignment of the angular momentum about the cranking axis. After $\omega_{\rm rot} \approx 0.6$ MeV/$\hbar$, there are many quasiparticles, both proton and neutron ones, crossing the zero energy, which changes the configurations of the yrast and near yrast states and also affects the result of the RPA calculations.

In the following we will show the result of calculations mainly for ^{163}Lu, for which most complete experimental data are available.

Next we compare the calculated and measured cranking moment of inertia for the yrast TSD band of ^{163}Lu in Fig. 3, and those of in-band $B(E2)$ in Fig. 4, respectively, as functions of the rotational frequency. Here we use the standard procedure[76] ($K = 1/2$ is assumed to transform the total angular momentum quantum number to the aligned angular momentum) for obtaining the measured cranking moment of inertia. For the calculation in these figures all the mean-field parameters are assumed to be constants, $(\beta_2, \gamma, \beta_4) = (0.42, 18^\circ, 0.02)$ and $\Delta_\pi = \Delta_\nu = 0.5$ MeV, as a typical example. Since the moment of inertia $\mathcal{J}_x$, defined in Eq. (2·30), i.e.,

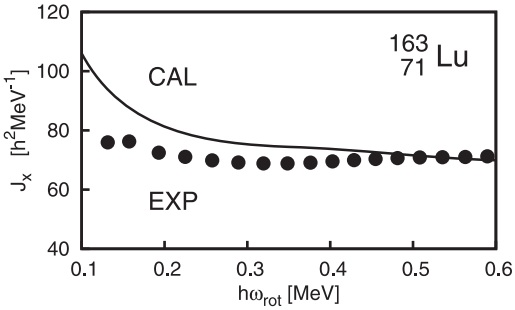

Fig. 3. The cranking moment of inertia $\mathcal{J}_x$ in Eq. (2·30) for ^{163}Lu as a function of the rotational frequency. The fixed deformation parameters $(\beta_2, \gamma, \beta_4) = (0.42, 18^\circ, 0.02)$ and the fixed pairing gaps $\Delta_\pi = \Delta_\nu = 0.5$ MeV are used. Experimental data are taken from Ref. 6).

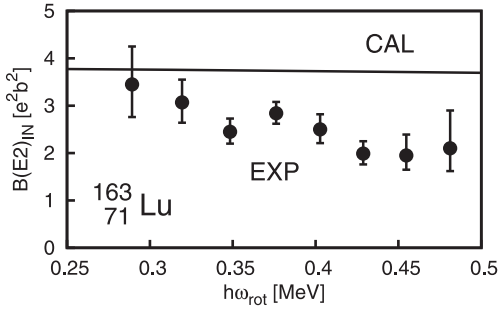

Fig. 4. The in-band $B(E2)$ calculated by Eq. (2·44) for ^{163}Lu as a function of the rotational frequency. The mean-field parameters are fixed and the same as in Fig. 3. Experimental data are taken from Ref. 16).

the so-called kinematic moment of inertia, contains the contribution of quasiproton alignment, $\approx i/\omega_{\rm rot}$ (where i is the aligned angular momentum), the calculated $\mathcal{J}_x$ decreases as $\omega_{\rm rot}$ increases, if all the mean-field parameters are fixed. In contrast the measured inertia is almost constant against the change of the rotational frequency, suggesting at least one (or some) of the mean-field parameters is actually varying. The recently measured lifetimes of the TSD band[16] indicate that the experimental in-band $B(E2)$, on the other hand, decreases rather rapidly, while the calculated in-band $B(E2)$ is almost constant reflecting that the constant deformation parameters are used in this calculation. Therefore the $B(E2)$ data also suggest that at least one (or some) of the deformation parameters is changing as a function of $\omega_{\rm rot}$. This behavior of the in-band $B(E2)$ as well as out-of-band $B(E2)$ will be discussed in more detail in the following §3.5.

3.2. *RPA calculations*

Once the nuclear mean-field is specified and the cranked quasiparticles, Eq. (2·11), are obtained, it is straightforward to solve the RPA equation, Eq. (2·24), or equivalently, Eq. (2·33) for the non-NG modes. It should be mentioned that the vacuum mean-field state of the RPA excitations is the lowest quasiproton excited state for the odd-Z nucleus ^{163}Lu; such a state can be obtained by exchanging the HFB wave function and energy[27] of the excited quasiproton orbital to the opposite signature sector $(U, V, E) \to (\bar{V}, \bar{U}, -\bar{E})$. The details of the procedure to perform the RPA on such excited configurations are explained in Ref. 45), where the RPA excitations on the two quasineutron configuration (the Stockholm band) were treated. At the ground state ($\omega_{\rm rot} = 0$) any one quasiparticle configuration has the Kramers degeneracy so that it cannot be selected as a vacuum of the RPA, but at finite rotational frequency the degeneracy is lifted and then it is possible to perform the RPA calculation without any problems.

Since it is guaranteed in our formalism that the NG mode solution $\omega_{n=\rm NG} = \omega_{\rm rot}$

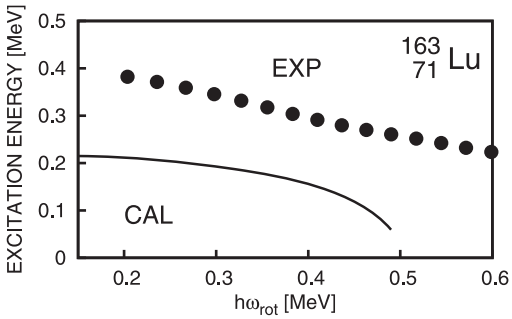

Fig. 5. The eigenenergy of the wobbling-like RPA solution as a function of the rotational frequency. The mean-field parameters are fixed and the same as in Fig. 3. Experimental data are taken from Ref. 6).

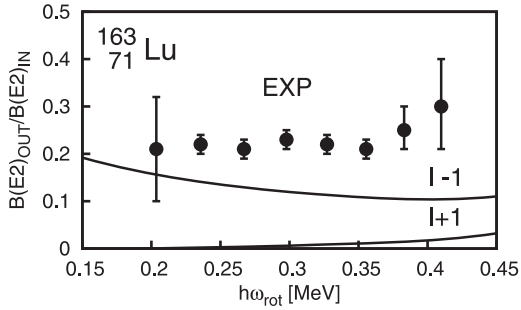

Fig. 6. The out-of-band to in-band $B(E2)$ ratio. The ratios associated with the $I \to I \pm 1$ out-of-band transitions are depicted as separate lines with the attached labels $I \pm 1$. The mean-field parameters are fixed and the same as in Fig. 3. Experimental data are taken from Ref. 16), in which only the $I \to I - 1$ transitions are measured.

is precisely given by Eq. (2·18), we actually solve Eq. (2·33) to obtain the non-NG eigenenergy ω_n and the amplitude $(\chi_y \mathcal{F}_y(n), \chi_z \mathcal{F}_z(n))$, and then its forward and backward amplitudes are given by Eq. (2·22). As is mentioned in the previous section, it is important to use a sufficient model space in the RPA calculation for the consistent description of the NG mode (2·18). We have checked that the full use of the oscillator shells up to $N_{\max} = 12$ is enough: Then the total number of proton and neutron two quasiparticle states (α, β) is about 210,000 for the signature $(-)$ RPA calculation. Using the formulation explained in the previous section, we have performed the Woods-Saxon RPA calculation, and found, just like in the previous Nilsson calculations,[46)–48)] that the RPA modes that satisfy the requirements of the wobbling motion exist systematically in the TSD configurations.

As an example, the excitation energy of the wobbling-like RPA solution in ^{163}Lu is compared with the experimental data in Fig. 5. In this calculation the constant mean-field parameters are used just like in Figs. 3 and 4. The calculated excitation energy vanishes at a finite frequency, in this example about 0.5 MeV/$\hbar$, which is mainly due to the fact that many quasiparticle states come close to zero energy and the vacuum configuration changes as is seen in Fig. 2. The out-of-band $B(E2)$ calculated by Eqs. (2·39) and (2·41) is an important quantity to identify the wobbling motion, which is as large as about 100 Weisskopf units. In experiments the out-of-band to in-band $B(E2)$ ratio, $B(E2, I \to I-1)_{\rm out}/B(E2, I \to I-2)_{\rm in}$ has been directly measured, and we compare the result of RPA calculation with experimental data for this ratio in Fig. 6.

It should be noted that only the $I \to I - 1$ transitions are measured for the out-of-band transitions, which suggests that the $I \to I + 1$ out-of-band transitions are small and indicate the positive γ shape. This characteristic behavior of the rotor model also exists in the microscopic RPA calculation.[42)] From Eqs. (2·39) and (2·41)

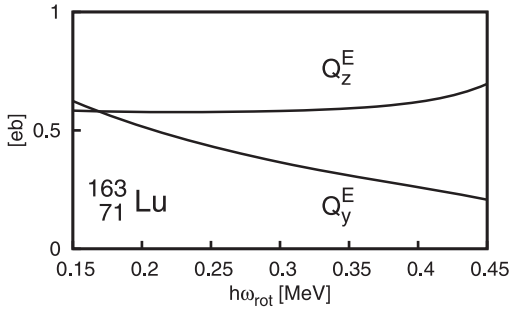

Fig. 7. The calculated quadrupole amplitudes $\mathcal{Q}^E_{y,z}(n = \text{wob})$ in Eq. (3·2) of the wobbling-like RPA solution as functions of the rotational frequency.

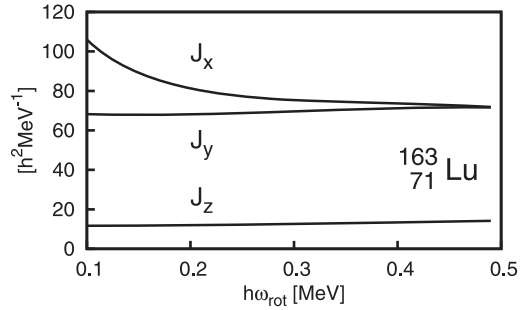

Fig. 8. The three moments of inertia, $\mathcal{J}_x$ and $\mathcal{J}^{\text{eff}}_{y,z}(n = \text{wob})$ as functions of the rotational frequency. The mean-field parameters are fixed and the same as in Fig. 3.

the out-of-band $B(E2)$ of the n-th RPA phonon excited state is

$$B(E2; In \to I \pm 1\text{vac}) \approx \frac{1}{2}\big(\mathcal{Q}^E_y(n) \mp \mathcal{Q}^E_z(n)\big)^2. \tag{3·2}$$

The electric quadrupole matrix elements $\mathcal{Q}^E_y(n)$ and $\mathcal{Q}^E_z(n)$ have the same sign and comparative magnitude for the wobbling-like solution ($n = \text{wob}$) for the positive γ shape, as they are depicted in Fig. 7. Thus the $I \to I-1$ transitions are much more enhanced than the $I \to I+1$ transitions. In Fig. 6 the $B(E2)$'s of both transitions are shown; that of the $I \to I+1$ transitions is smaller by an order of magnitude or more.

The calculated energy of the wobbling excitation is 100−200 keV smaller than the experimental data; this trend seems general and is similar in the previous Nilsson RPA calculations.[46)–48)] It is pointed out in Refs. 23) and 24) that the particle-rotor coupling increases the excitation energy of the wobbling phonon considerably: $\Delta\omega_{\text{p-wob}} \approx j/\mathcal{J}_x$ in a simple limiting approximation,[23)] where j is the angular momentum of the coupled quasiparticle, $j = 13/2$, so that $\Delta\omega_{\text{p-wob}} \approx 90$ keV in the case of ^{163}Lu. In our microscopic calculation the effect of the particle-rotor coupling is partly taken into account as a kind of blocking effect; the vacuum of the RPA excitation contains the odd quasiproton in the calculation. However, there exist explicit coupling effects between the RPA phonon and an odd quasiparticle. The underestimation of the wobbling excitation energy in odd-Z Lu nuclei in the present and the previous RPA calculations may be due to this reason. More detailed theoretical investigations of the RPA-phonon-quasiparticle coupling calculation, see e.g. Ref. 77), are necessary to draw a definite conclusion to this point.

Although the calculated out-of-band to in-band $B(E2)$ ratio in the present Woods-Saxon RPA calculation is about 10−20% larger than the previous Nilsson RPA calculation, it is still considerably smaller than the experimental data on average. Moreover, in contrast to the almost constant ratio of the experimental data, the calculated $B(E2)$ ratio is decreasing as a function of the rotational frequency. Thus, the basic trend is similar to the previous Nilsson calculations, and was a most serious problem of the microscopic calculation compared with the macroscopic rotor model.

It is, however, found that the problem of underestimation is due to the inconsistent definition of the triaxiality parameter "γ" in the mean-field potential (either Nilsson or Woods-Saxon) and in the macroscopic model.[55] These characteristic features of the calculated and measured $B(E2)$ will be discussed in more detail in §3.5.

Now let us discuss the results of calculation transformed into the PA frame. The three moments of inertia corresponding to the wobbling-like solution in Fig. 5 are shown in Fig. 8. The $\mathcal{J}_x$ inertia is the same as in Fig. 3. Other inertias, $\mathcal{J}_y^{\rm eff}$ and $\mathcal{J}_z^{\rm eff}$, are calculated according to Eq. (2·63) not to Eq. (2·36); the results of these two equations are different for the general mean-field potential. We have found, however, that the actual numerical difference between the two definitions is small, within 1% at least in the present calculation; this suggests that the operators $F_{y,z}$ in Eq. (2·8) obtained with the present Woods-Saxon mean-field are not so much different from those proportional to the quadrupole operators $Q_{y,z}$ in Eq. (2·14). The calculated inertias $\mathcal{J}_{y,z}^{\rm eff}$ are almost constant in this calculation with fixed mean-field parameters, and $\mathcal{J}_y^{\rm eff}$ is much larger than $\mathcal{J}_z^{\rm eff}$. These basic features are similar to the previous Nilsson RPA calculations.[46] We also show, in Fig. 9, the wobbling angles of the angular momentum vector in the PA frame (c.f., Eqs. (2·54), (2·57) and (2·58)), which are defined for the n-th RPA mode by[53),54]

$$\begin{aligned} \tan\theta(n) &\equiv \frac{\sqrt{(J_y)_{\rm PA}(n)^2+(J_z)_{\rm PA}(n)^2}}{\langle J_x\rangle} = \sqrt{r_y^2(n)+r_z^2(n)}, \\ \tan\psi(n) &\equiv \frac{(J_z)_{\rm PA}(n)}{(J_y)_{\rm PA}(n)} = \frac{r_y(n)}{r_z(n)}, \end{aligned} \tag{3·3}$$

for which the small amplitude approximation requires $\tan\theta(n)\approx\theta(n)$. From this figure the angle θ is about 25° (0.44 radian), and the small amplitude approximation may be acceptable. Note that the quantities $r_y(n)$ and $r_z(n)$ describe the shape fluctuations in the UR frame, Eq. (2·57), and, at the same time, the angular momentum fluctuations in the PA frame, Eq. (2·58); $r_y(n)<r_z(n)$ in this calculation and $r_y(n)$ decreases as a function of $\omega_{\rm rot}$, and becomes $r_y(n)\ll r_z(n)$ at higher frequency (c.f., Fig. 7). This means that the angular momentum fluctuation of the y-direction is much larger than that of the z-direction, and so the angle $\psi\to 0$ in Fig. 9.

Finally, the calculated out-of-band $B(M1)$ to in-band $B(E2)$ ratio is compared with the experimental data in Fig. 10 as in the same way as the $B(E2)$ ratio, but in the log scale. The $B(M1)$ transition is calculated by Eqs. (2·40) and (2·42), i.e.,

$$B(M1; In\to I\pm 1{\rm vac}) \approx \frac{1}{2}\big(\mu_y(n)\pm\mu_z(n)\big)^2, \tag{3·4}$$

where the RPA matrix elements of the $M1$ operator are given in the same way as those of $E2$ operator,

$$\mu_y(n)\equiv\langle[X_n,i\mu_y]\rangle, \quad \mu_z(n)\equiv\langle[X_n,\mu_z]\rangle. \tag{3·5}$$

The effective spin g-factor $g_s^{\rm eff}=0.6\,g_s^{\rm free}$ is used;[6),22] we have checked that the result with using $g_s^{\rm eff}=0.7\,g_s^{\rm free}$ does not change essentially. The $I\to I-1$ transitions are larger than the $I\to I+1$ transitions by factor two to four, in contrast

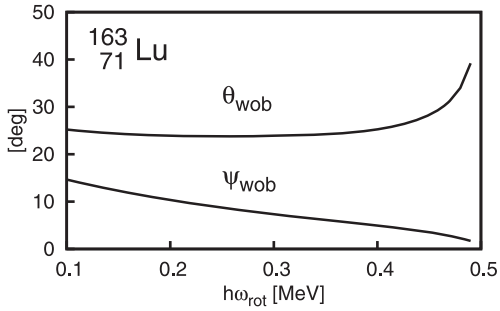

Fig. 9. The wobbling angles of the angular momentum vector in the PA frame for the RPA wobbling excitation, $\theta(n = \text{wob})$ and $\psi(n = \text{wob})$, defined in Eq. (3·3), as functions of the rotational frequency.

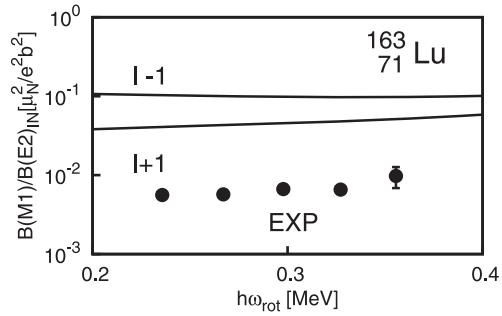

Fig. 10. The out-of-band $B(M1)$ to in-band $B(E2)$ ratio. Both the $I \to I \pm 1$ transitions are depicted as separate lines with the attached labels $I \pm 1$. Note that the ratios are drawn in a log scale. The mean-field parameters are fixed and the same as in Fig. 3. Experimental data are taken from Ref. 3), in which only the $I \to I - 1$ transitions are measured.

to the case of $B(E2)$ ratio. This is because the $\mu_y(n)$ amplitude is much larger than the $\mu_z(n)$ at all rotational frequencies in the present calculation. As shown in Fig. 10, the calculated ratio is about one order of magnitude larger than the experimental data, which is similar to that of Ref. 49). The relative sign of the matrix elements between the $E2$ and $M1$ transitions is negative, which agrees with the experimentally measured $E2/M1$ mixing ratio.[1),6)] As for the $B(M1)$ ratio, the measured values[3)] are 0.0056 $[\mu_N^2/e^2b^2]$ at lower spins and 0.0098 at higher spins. The particle-rotor model calculations[1),24)] give about 0.015−0.02 at lower spins and about 0.01 at higher spins. In the previous Nilsson RPA calculation,[46)] the corresponding values are about 0.04 and 0.015. Compared with these other calculations, our present value of $B(M1)$ is too large, about 0.1, and almost constant, while the other calculations predict that the $B(M1)$ ratio decreases as a function of ω_{rot}. We do not understand the reason why the present Woods-Saxon RPA calculation gives larger values especially at higher spin than the previous Nilsson RPA calculation. It should be mentioned that the absolute value of the $B(M1)$ is small compared to the Weisskopf unit, but still it is much larger than the experimental data. This means that the RPA eigenmode operator corresponding to the wobbling excitation should be almost completely orthogonal to the $M1$ operator (2·42), i.e., the various orbital contributions should cancel out, in order to obtain the agreement with the experimental data; the cancellation is not enough in the present calculation. Since our calculation does not agree with experimental data for $B(M1)$, we concentrate on the excitation energy and $B(E2)$ in the following further investigations.

3.3. *Dependence on mean-field parameters*

Until now we have shown the results of the microscopic calculations with fixed mean-field parameters at the reference values, $(\beta_2, \gamma, \beta_4) = (0.42, 18^\circ, 0.02)$ and $\Delta_\pi =$

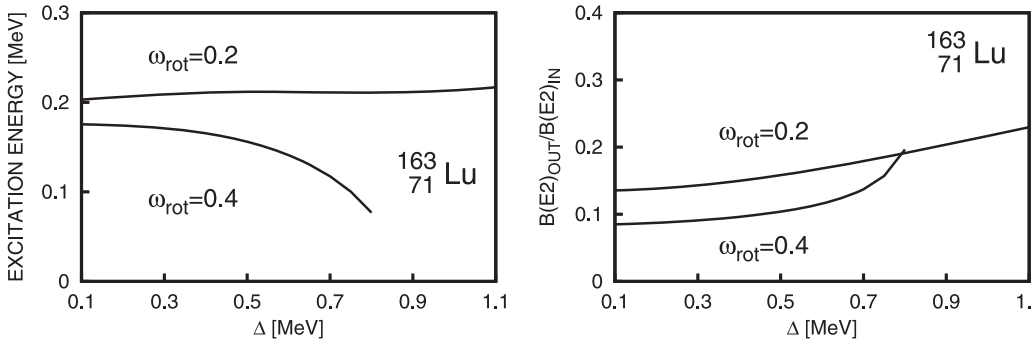

Fig. 11. Dependence of the eigenenergy (left panel) or of the out-of-band to in-band $B(E2)$ ratio (right panel) on the pairing gap $\Delta = \Delta_\pi = \Delta_\nu$ for the wobbling-like RPA solution. The two curves correspond to the results at $\omega_{\rm rot} = 0.2$ and 0.4 MeV/$\hbar$. The mean-field parameters except the pairing gaps are the same as in Fig. 3.

$\Delta_\nu = 0.5$ MeV. As it is explained in §3.1, we do not know very well about what are the best values for these parameters. They might change depending on the rotational frequency, and then it must be clarified how their dependences are; for example, it is well-known that the proton and neutron pairing gaps should decrease as functions of the rotational frequency because of the Coriolis anti-pairing effect. Instead of looking for what should be the values of these mean-field parameters, we here discuss how the results of the present Woods-Saxon RPA calculation change when these mean-field parameters are varied in a reasonable range.

First, we show the dependence of the wobbling excitation energy and the $B(E2)$ ratio on the pairing gap, $\Delta \equiv \Delta_\pi = \Delta_\nu$, i.e., the proton and neutron gaps being set equal for simplicity, in Fig. 11. In these figures, those at the rotational frequencies, $\omega_{\rm rot} = 0.2$ and 0.4 MeV/$\hbar$ are shown. As it is clear the dependence of the wobbling excitation energy on the pairing gap is rather weak, and the very collective RPA solution exists even in the $\Delta = 0$ limit; at higher frequency $\omega_{\rm rot} = 0.4$ MeV/$\hbar$ near the critical frequency of vanishing RPA energy, $\omega_{\rm rot} \approx 0.5$ MeV/$\hbar$, the solution becomes unstable for larger pairing gaps. This is in contrast to the collective vibrational mode, and discussed[46),48),65)] to be the characteristic property of the wobbling mode, which is of rotational origin. The dependence of the $B(E2)$ ratio on Δ, which comes solely from the out-of-band $B(E2)$, is slightly stronger, but again, smaller than that of the collective vibrational mode. The dependences of the cranking moment of inertia and the in-band $B(E2)$ are well-known: The cranking moment of inertia decreases by about 27% (15%) at $\omega_{\rm rot} = 0.2$ (0.4) MeV/$\hbar$ as Δ increases from 0.1 to 0.8 MeV for ^{163}Lu (not shown), while the in-band $B(E2)$ does not depend on Δ essentially.

Next, we show the dependence of the wobbling excitation energy and the $B(E2)$ ratio on the magnitude of deformation β_2 in Fig. 12. Other parameters are fixed at the reference values. The excitation energy slightly depends on β_2 but is stable in the calculated range. The $B(E2)$ ratio is almost independent of β_2; this is quite reasonable in the macroscopic model, because both the in-band $B(E2)$ and out-of-band $B(E2)$ depend on the square of magnitude of deformation and it cancels when their ratio is taken. The in-band $B(E2)$ increases monotonically as β_2 increases

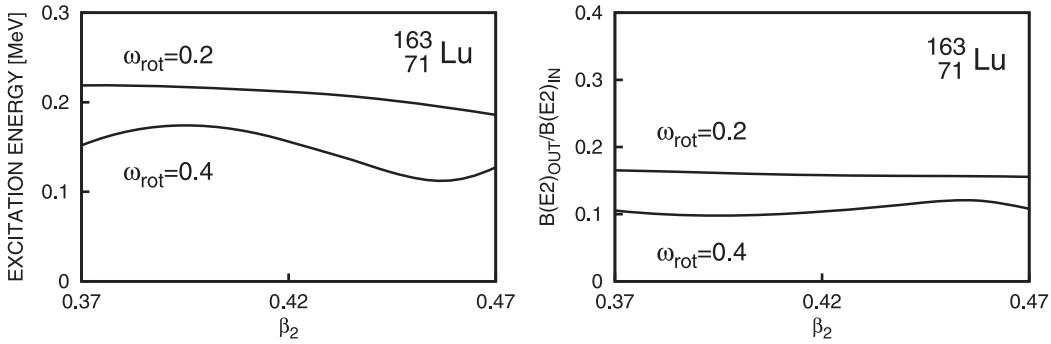

Fig. 12. Dependence of the eigenenergy (left panel) or of the out-of-band to in-band $B(E2)$ ratio (right panel) on the deformation parameter β_2 for the wobbling-like RPA solution. The two curves correspond to the results at $\omega_{\rm rot} = 0.2$ and 0.4 MeV/$\hbar$. The mean-field parameters except β_2 are the same as in Fig. 3.

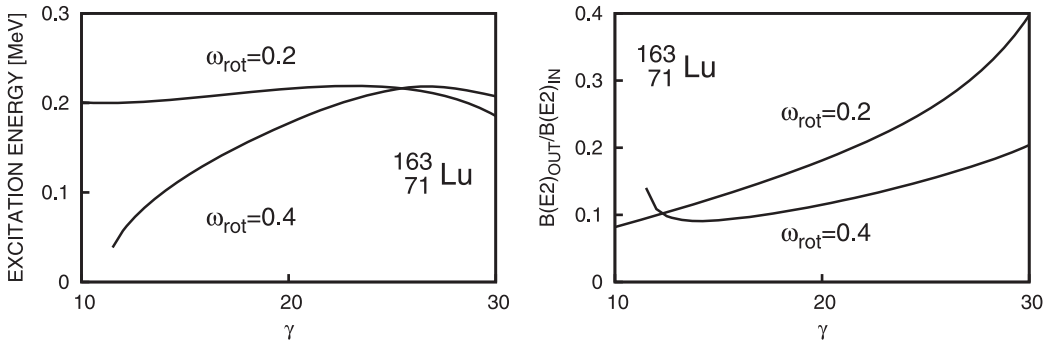

Fig. 13. Dependence of the eigenenergy (left panel) or of the out-of-band to in-band $B(E2)$ ratio (right panel) on the deformation parameter γ for the wobbling-like RPA solution. The two curves correspond to the results at $\omega_{\rm rot} = 0.2$ and 0.4 MeV/$\hbar$. The mean-field parameters except γ are the same as in Fig. 3.

with keeping γ (not shown), because the intrinsic quadrupole moment about the x-axis increases. However, the cranking moment of inertia $\mathcal{J}_x$ is almost constant or slightly decreases (not shown); this is because the core contribution increases but the quasiproton alignment contribution decreases and these two almost cancel.

Finally, we show the dependence of the wobbling excitation energy and the $B(E2)$ ratio on the triaxiality parameter γ in Fig. 13. Again, the excitation energy slightly depends on γ but is stable in the range, $15^\circ < \gamma < 30^\circ$. On the other hand, the $B(E2)$ ratio increases rapidly as γ increases. Both the in-band $B(E2)$ and out-of-band $B(E2)$ depend on the triaxiality in definite ways according to the macroscopic model. The result of the microscopic RPA calculation reproduces the characteristic features of the rotor model rather well, and this is precisely the reason that we can identify the obtained RPA solution as the wobbling excitation mode. The in-band $B(E2)$ decreases monotonically as γ increases (not shown, but see §3.5). The cranking moment of inertia slightly increases (not shown); the core contribution

decreases but the quasiproton alignment contribution increases, and the alignment contribution slightly wins in the present case.

3.4. *Calculation with varying pairing gaps*

The mean-field parameters are kept constants against the change of the rotational frequency in the results presented above. However, at least the proton and neutron pairing gaps should decrease as functions of the rotational frequency due to the Coriolis anti-pairing effect. Therefore, it is desirable to determine Δ_π and Δ_ν selfconsistently. For this purpose, we fix the pairing force strength at the ground state with the pairing model space explained in §3.1, by

$$G_\tau = \Delta_\tau(\mathrm{eo})/\langle P_\tau \rangle_{\mathrm{gr}}, \tag{3·6}$$

and use this strength for the TSD bands. Here $\Delta_\tau(\mathrm{eo})$ is the experimental even-odd mass difference evaluated by the third order difference formula,[5] and $\langle P_\tau \rangle_{\mathrm{gr}}$ is the expectation value of the monopole pair transfer operator with respect to the normal deformed ground state ($\omega_{\mathrm{rot}} = 0$), whose deformation is obtained by the Woods-Saxon Strutinsky calculation; i.e., $\beta_2 = 0.217, \gamma = 0, \beta_4 = -0.002$ for ^{163}Lu.

The same Strutinsky calculation for the ground state, where the smooth pairing gap method is used with $\widetilde{\Delta} = 13/\sqrt{A}$ MeV, gives the pairing gaps, $\Delta_{\pi,\mathrm{gr}} = 0.839$ MeV and $\Delta_{\nu,\mathrm{gr}} = 1.233$ MeV for ^{163}Lu. It should be noted, here, that the situation is puzzling: the even-odd mass differences for ^{163}Lu are $\Delta_\pi(\mathrm{eo}) = 1.243$ MeV and $\Delta_\nu(\mathrm{eo}) = 0.868$ MeV by using the 1995 mass data.[78] In the neighboring even-even nuclei, $\Delta_\pi(\mathrm{eo}) = 1.180$ MeV and $\Delta_\nu(\mathrm{eo}) = 1.167$ MeV for ^{162}Yb, and $\Delta_\pi(\mathrm{eo}) = 1.260$ MeV and $\Delta_\nu(\mathrm{eo}) = 1.221$ MeV for ^{164}Hf. Taking into account the blocking effect, the calculated pairing gaps ($\Delta_{\pi,\mathrm{gr}} = 0.839$ MeV and $\Delta_{\nu,\mathrm{gr}} = 1.233$ MeV) are reasonable in comparison with the even-odd mass differences of neighboring even-even nuclei. However, $\Delta_\pi(\mathrm{eo})$ in ^{163}Lu is too large while $\Delta_\nu(\mathrm{eo})$ is too small compared with those in the neighboring even-even nuclei. This trend is not particular in ^{163}Lu, but it seems general in odd-proton nuclei in this rare earth region, for which we do not know the reason yet. In Ref. 60), we have used the neutron or proton pairing force strength which is an average of those for the neighboring even-even nuclei determined by the even-odd mass differences. In order to confirm that the results are not very different from those of Ref. 60), we use, in the present work, the pairing force strengths determined by the even-odd mass differences of ^{163}Lu.

By using the pairing force strengths thus determined, we have done selfconsistent pairing calculation with the deformation parameters fixed at the reference value $(\beta_2, \gamma, \beta_4) = (0.42, 18°, 0.02)$. Then the proton and neutron pairing gaps vanish at $\omega_{\mathrm{rot}} \approx 0.42$ and 0.43 MeV/$\hbar$, respectively, due to the alignments of quasiparticles. The abrupt pairing collapse is a drawback of the mean-field approximation, and we use the following phenomenological parameterization at finite rotational frequency,[79]

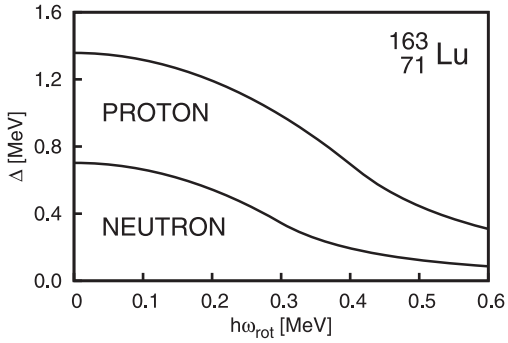

Fig. 14. The proton and neutron pairing gaps used in the pairing varied calculation as functions of the rotational frequency for ^{163}Lu. The deformation parameters used are $(\beta_2, \gamma, \beta_4) = (0.42, 18^\circ, 0.02)$.

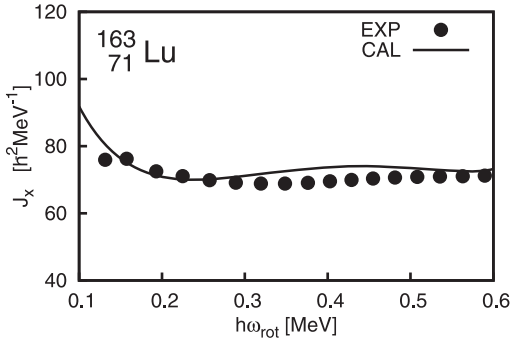

Fig. 15. The cranking moment of inertia as a function of the rotational frequency. The deformation parameters are fixed but the pairing gaps in Fig. 14 are used.

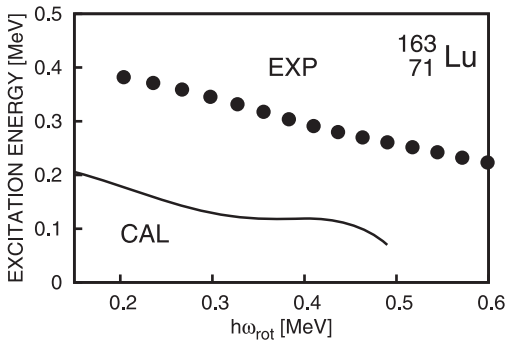

Fig. 16. The eigenenergy of the wobbling-like solution as a function of the rotational frequency. The deformation parameters are fixed but the pairing gaps in Fig. 14 are used.

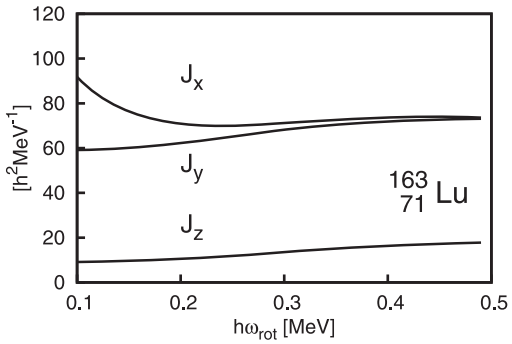

Fig. 17. The three moments of inertia, $\mathcal{J}_x$ and $\mathcal{J}^{\rm eff}_{y,z}(n = \text{wob})$ as functions of the rotational frequency. The deformation parameters are fixed but the pairing gaps in Fig. 14 are used.

$$\Delta(\omega_{\rm rot}) = \Delta_0 \times \begin{cases} \left[1 - \frac{1}{2}\left(\frac{\omega_{\rm rot}}{\omega_{\rm c}}\right)^2\right], & \omega_{\rm rot} < \omega_{\rm c}, \\ \frac{1}{2}\left(\frac{\omega_{\rm c}}{\omega_{\rm rot}}\right)^2, & \omega_{\rm rot} \geq \omega_{\rm c}, \end{cases} \tag{3·7}$$

where the parameters $\Delta_0 = \Delta(\omega_{\rm rot} = 0)$ and ω_c, such that $\Delta(\omega_{\rm rot} = \omega_c) = \frac{1}{2}\Delta_0$, are determined by the selfconsistent pairing calculations. The resultant pairing gaps are shown in Fig. 14.

We have done the semi-phenomenological pairing selfconsistent calculation by using the pairing gaps in Fig. 14 and the constant deformation parameters at the reference values, $(\beta_2, \gamma, \beta_4) = (0.42, 18^\circ, 0.02)$. The result for the cranking moment of inertia is shown in Fig. 15. Comparing with the constant pairing calculation in

Fig. 3, the agreement between the experimental data and the calculation is much better. This means that the present Woods-Saxon RPA model can describe both the yrast TSD band and the wobbling excitation at the same time, which is a great advantage over the previous Nilsson RPA model, where the cranking moment of inertia is overestimated and the Strutinsky renormalization of the angular momentum is necessary to reproduce the yrast TSD band.

The result of the excitation energy of the RPA wobbling mode is compared with the experimental data in Fig. 16. The behavior of the excitation energy is not very different from the constant pairing calculation in Fig. 5, but the overall energy is slightly lower and about 200 keV smaller than the experimental data. The three moments of inertia in the PA frame calculated with varying pairing gaps are shown in Fig. 17. In contrast to the corresponding constant pairing calculation in Fig. 8, the inertias $\mathcal{J}^{\rm eff}_{y,z}$ acquire sizable dependence on the rotational frequency, but the basic features such as $\mathcal{J}^{\rm eff}_{y} \gg \mathcal{J}^{\rm eff}_{z}$ are almost the same. As for the $B(E2)$'s, the in-band $B(E2)$ and the out-of-band to in-band $B(E2)$ ratio are shown as solid lines in Figs. 18 and 19. As it is discussed in §3.3, the in-band $B(E2)$ does not depend on the pairing gaps, so the result is almost the same as that with the fixed mean-field parameters in Fig. 4. The $B(E2)$ ratio is slightly different from that in Fig. 6, but the difference is small. Thus, the calculation with varying pairing gaps is not helpful to fill the gap for the discrepancy between the calculation and the experimental data of $B(E2)$'s, which is considered in the next subsection.

3.5. $B(E2)$ *and triaxial deformation*

The out-of-band $B(E2)$ from the excited band to the yrast TSD band is the crucial quantity to identify the nuclear wobbling motion. The recent lifetime measurement of the excited and yrast TSD bands[15),16)] revealed that the out-of-band $B(E2)$ is as large as about 100 Weisskopf units, which is much larger than the typical collective-vibrational $E2$ transitions, and is possibly the largest interband $E2$ transitions. It is important not only to identify the wobbling excitation but also to deduce the triaxiality parameter γ; according to the rotor model, the out-of-band to in-band $B(E2)$ ratio directly reflects the triaxiality of the quadrupole deformation. Here it should be noted that there are various different definitions of the triaxiality parameter γ, and one should be careful which definition is used for quantitative discussions.[55)]

The parameter γ in the mean-field potential, Eq. (2·5), is one of such definitions, called γ(pot:WS) in Ref. 55), but it is different from the one specified by the quadrupole moments, which is called γ(den) and defined by

$$Q\cos\gamma \equiv \sqrt{\frac{16\pi}{5}}\,\langle Q^{(+)}_{20}\rangle, \quad Q\sin\gamma \equiv -\sqrt{\frac{16\pi}{5}}\,\langle Q^{(+)}_{22}\rangle, \tag{3·8}$$

where Q is the total quadrupole moment. In terms of this $\gamma = \gamma$(den), the quantities $\alpha_{y,z}R^2$ in Eq. (2·48) can be expressed as $\alpha_y R^2 = -\sqrt{\frac{5}{16\pi}}\,Q\sin(\gamma+60^\circ)$ and $\alpha_z R^2 = -\sqrt{\frac{5}{16\pi}}\,Q\sin\gamma$, and then by using Eq. (2·65) with (2·57) the out-of-band $B(E2)$ in

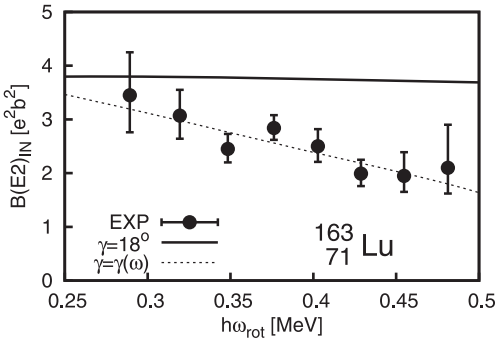

Fig. 18. The in-band $B(E2)$ defined for ^{163}Lu as a function of the rotational frequency (solid line). The deformation parameters are fixed but the pairing gaps in Fig. 14 are used. The dashed line is the result of calculation with further changing the γ parameter linearly from $\gamma = 18^\circ$ at $\omega_{\rm rot} = 0.2$ MeV/$\hbar$ to $\gamma = 30^\circ$ at $\omega_{\rm rot} = 0.4$ MeV/$\hbar$.

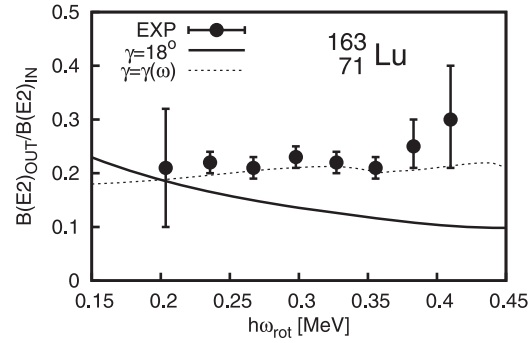

Fig. 19. The out-of-band to in-band $B(E2)$ ratio for ^{163}Lu as a function of the rotational frequency (solid line). The deformation parameters are fixed but the pairing gaps in Fig. 14 are used. The dashed line is the result of calculation with further changing the γ parameter linearly from $\gamma = 18^\circ$ at $\omega_{\rm rot} = 0.2$ MeV/$\hbar$ to $\gamma = 30^\circ$ at $\omega_{\rm rot} = 0.4$ MeV/$\hbar$. The $B(E2)$ ratio with only $I \to I - 1$ transitions is shown.

Eq. (3·2) is represented as in the same form as the macroscopic rotor expression,[5)]

$$B(E2; In \to I \pm 1\text{vac}) \approx \frac{5}{16\pi}\left(e\frac{Z}{A}Q\right)^2 \frac{1}{I}\left[\left(\frac{W_z(n)}{W_y(n)}\right)^{1/4}\sin(\gamma + 60^\circ) \mp \left(\frac{W_y(n)}{W_z(n)}\right)^{1/4}\sin\gamma\right]^2, \tag{3·9}$$

with the definitions

$$W_y(n) \equiv 1/\mathcal{J}_z^{\rm eff}(n) - 1/\mathcal{J}_x, \quad W_z(n) \equiv 1/\mathcal{J}_y^{\rm eff}(n) - 1/\mathcal{J}_x. \tag{3·10}$$

Here $\langle J_x \rangle \approx I$, $Q^E_{y,z} = (eZ/A)\, Q_{y,z}$, and $c_n^2 = 1$ as well as $\sigma = +$ in Eq. (2·66) are further assumed. As it is discussed in §2.3, the condition $c_n^2 = 1$ and $\sigma = +$ can be regarded as a requirement for the wobbling-like RPA solution: In the present and the previous calculations this condition is satisfied if the used model space is large enough to guarantee the exact NG mode decoupling; the deviation is within 2% in the present calculations. Using the same $\gamma = \gamma(\text{den})$ and the assumption $Q^E_{2\nu} = (eZ/A)Q_{2\nu}$, the in-band $B(E2)$ in Eq. (2·44) can be also expressed as

$$B(E2; I \to I \pm 2) \approx \frac{5}{32\pi}\left(e\frac{Z}{A}Q\right)^2 \cos^2(\gamma + 30^\circ). \tag{3·11}$$

In this way, the out-of-band to in-band $B(E2)$ ratio does not depend on the total quadrupole moment Q (and so not on β_2 and β_4) in a good approximation, and the decreasing trend of the calculated $B(E2)$ ratio as a function of the rotational frequency can be naturally understood by the $1/I$ factor in Eq. (3·9).

It should be emphasized that the γ parameter appearing in Eqs. (3·9) and (3·11), which are essentially the formula employed in the particle-rotor model calculations[22)–25)] (note that the effect of the odd particle is negligible for $B(E2)$'s), is $\gamma = \gamma(\text{den})$ in Eq. (3·8) and not $\gamma(\text{pot:WS})$ in Eq. (2·5). As it is demonstrated in Ref. 55), they are rather different at a given shape especially for larger quadrupole deformations; for example, $\gamma(\text{den}) = 20^\circ$ corresponds to $\gamma(\text{pot:WS}) \approx 30^\circ$, for the TSD shape of the Lu and Hf region (see Fig. 4 of Ref. 55)). It was discussed in the particle-rotor model calculations[22),23)] that $\gamma(\text{den}) \approx 20^\circ$ are necessary in order to reproduce the experimental $B(E2)$ ratio on average. This means that one has to use $\gamma \approx 30^\circ$ in the Woods-Saxon potential in Eq. (2·5). Since the calculated $B(E2)$ ratio increases as a function of the parameter γ as is discussed in §3.3, we obtain similar amount of agreement to that in the particle-rotor model if the increased value $\gamma \approx 30^\circ$ is used: This is demonstrated for the Nilsson RPA calculation in Ref. 55).

Although the average magnitude is improved by increasing the triaxiality of the mean-field, there is still considerable disagreement between the calculated and measured $B(E2)$ ratios: Their rotational frequency dependences are different. This suggests that some parameter of the mean-field should change as a function of the rotational frequency. Here it should be mentioned that the measured in-band $B(E2)$ also depends on the rotational frequency; it decreases as $\omega_{\rm rot}$ increases. This trend can be understood either as a result of decreasing β_2 (β_4) or as a result of increasing γ (or both of them). However, the $B(E2)$ ratio is almost independent of β_2 (β_4). Therefore, a simplest way to understand both $B(E2)$ data is to increase γ as a function of $\omega_{\rm rot}$. In the present work, we try to reproduce the $B(E2)$ data by varying the γ parameter linearly from $\gamma = 18^\circ$, i.e., $\gamma(\text{den}) \approx 12^\circ$, at $\omega_{\rm rot} = 0.2$ MeV/$\hbar$ to $\gamma = 30^\circ$, i.e., $\gamma(\text{den}) \approx 22^\circ$, at $\omega_{\rm rot} = 0.4$ MeV/$\hbar$. The results are shown as dashed lines in Figs. 18 and 19, where rather good agreements for both the in-band $B(E2)$ and the $B(E2)$ ratio are obtained. Considering that the various Nilsson Strutinsky calculations,[14)] including ours, predict that the triaxiality parameter does not change so largely, we need to look for more reliable methods to determine the mean-field parameters if this amount of change of the triaxial deformation is really true.

3.6. *Systematic calculations in Lu and Hf nuclei*

Until now we have considered only the nucleus ^{163}Lu as a best example. However, the wobbling excitations have been identified in several neighboring isotopes, ^{161}Lu,[10)] ^{165}Lu,[8)] and ^{167}Lu.[9)] Moreover, as it was predicted,[11),12),14)] the many possible candidates of the TSD bands have been observed in even-even Hf isotopes.[17)–21)] Therefore, it is interesting to know that the existence of the wobbling excitation is specific for the observed Lu isotopes or a general phenomenon. In our microscopic RPA formalism, the wobbling mode is a collective excitation mode like the low-lying collective vibrations, the β- or γ-vibrations, which are well-known to exist systematically near the ground states in the wide range of the periodic table. It can be inspected that the wobbling-like RPA solutions will be found generally in TSD nuclei. Thus, we have performed systematic RPA calculations for several Lu and Hf isotopes with $N = 90 - 96$. Although the mean-field parameters must be different in each isotope, we cannot determine them so that we have used for all nuclei the fixed

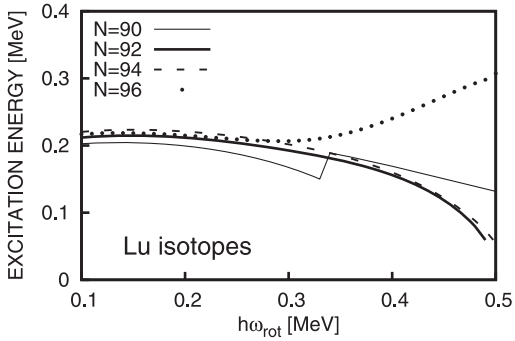

Fig. 20. The eigenenergies of the wobbling-like RPA solutions in Lu isotopes ($Z = 71$) with N =90, 92, 94, and 96 as functions of the rotational frequency. The mean-field parameters are fixed and the same as in Fig. 3.

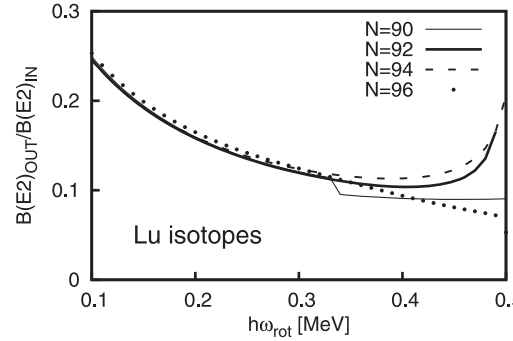

Fig. 21. The out-of-band to in-band $B(E2)$ ratios in Lu isotopes with N =90, 92, 94, and 96 as functions of the rotational frequency. The mean-field parameters are fixed and the same as in Fig. 3.

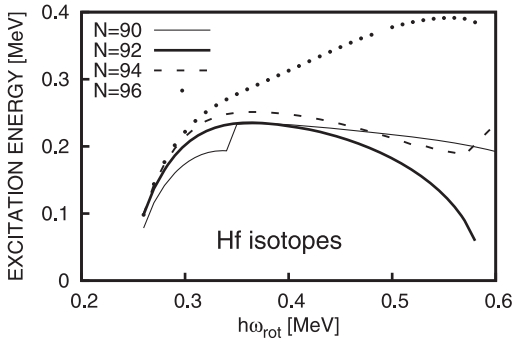

Fig. 22. The eigenenergies of the wobbling-like RPA solutions in Hf isotopes ($Z = 72$) with N =90, 92, 94, and 96 as functions of the rotational frequency. The mean-field parameters are fixed and the same as in Fig. 3.

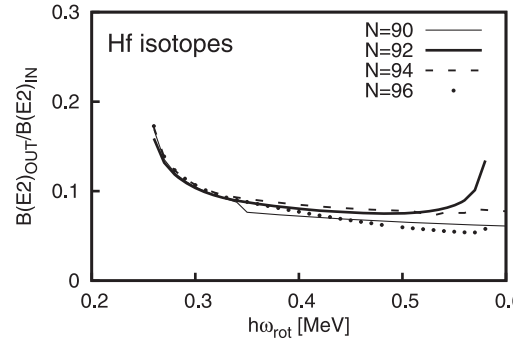

Fig. 23. The out-of-band to in-band $B(E2)$ ratios in Hf isotopes with N =90, 92, 94, and 96 as functions of the rotational frequency. The mean-field parameters are fixed and the same as in Fig. 3.

reference values that are used for ^{163}Lu in §3.2, i.e., $(\beta_2, \gamma, \beta_4) = (0.42, 18^\circ, 0.02)$ and $\Delta_\pi = \Delta_\nu = 0.5$ MeV. The results are shown in the four figures: The wobbling excitation energies of the Lu and Hf isotopes are shown in Figs. 20 and 22, and the out-of-band to in-band $B(E2)$ ratios of the Lu and Hf isotopes in Figs. 21 and 23, respectively.

As it is clear in these figures, the obtained wobbling excitation energies of Hf isotopes (about 220 keV) are slightly higher than those of Lu isotopes (about 180 keV), but those in each of the isotopes are rather similar with the exception of $N = 96$ isotopes, whose excitation energies increase by about 100−200 keV in $\omega_{\rm rot} > 0.3$ MeV/$\hbar$. The reason why the excitation energies increase in the $N = 96$ isotopes is that an additional two quasineutron alignment occurs gradually around that rota-

tional frequency in this particularly chosen mean-field parameters. We think that it is not so meaningful; in fact the observed wobbling excitation energy in ^{167}Lu is very similar to that in ^{163}Lu, and we have checked that the slight modification of the deformation parameters changes this trend of increasing energy of the $N = 96$ isotopes. The small kinks of $N = 90$ isotopes at $\omega_{\rm rot} \approx 0.32-0.35$ MeV/$\hbar$ are caused by a sharp crossing of two quasineutrons, whose orbital has rather small alignment and affects the vacuum very little. This is also a kind of artifact due to the mean-field parameters used presently, since the sharp crossing is not observed in experiment for the ^{161}Lu isotope. The $B(E2)$ ratios in the Lu and Hf isotopes are also very similar, again except for $N = 96$ isotopes, whose $B(E2)$ reduces slightly at higher rotational frequency due to the quasineutron alignment. In the Lu isotopes, the odd high-j ($N_{\rm osc} = 6$) quasiproton is always occupied. On the other hand the vacuum states are zero quasiproton states in the Hf isotopes, and the lowest two quasiprotons align at $\omega_{\rm rot} \approx 0.23$ MeV/$\hbar$ with relatively large interactions. As it is discussed in Refs. 46) and 48), the proton quasiparticle alignment is an important factor to stabilize the RPA wobbling excitation for the positive γ shape, so that the wobbling-like solutions appear only after the two quasiproton alignment in the Hf isotopes.

It must be emphasized that the collective RPA excitations exist irrespective of the proton number being odd or even in our microscopic RPA formalism. Therefore, the wobbling excitations should be identified also in the even-even Hf nuclei. It is mysterious for us that there has been no experimental sign of them in any Hf isotopes: This may suggest that some important elements may be still missing, which we do not know yet.

§4. Summary

We have investigated the nuclear wobbling motion in the Lu and Hf region by using the microscopic framework but in the small amplitude approximation, i.e., the cranked mean-field and the random phase approximation (RPA). The concept of the wobbling motion is intimately connected to the rotor model: The body-fixed frame or the principal-axis (PA) frame, where the degrees of freedom corresponding to the collective rotations are eliminated, plays a key role. In the conventional description, i.e., in the uniformly rotating (UR) frame of the cranking prescription, in which no concept of the body-fixed frame is introduced, the wobbling excitation is just like a usual collective vibration; only after transforming into the PA frame it can be interpreted as a motion of the angular momentum vector wobbling about the main rotation axis. Therefore, we reviewed the microscopic RPA framework,[32] where the PA frame is introduced, from a slightly general view point:[42] The original framework by Marshalek[32] assumes that the deformation of the mean-field is purely of quadrupole type, but such a limitation should be lifted for general mean-field potentials. By introducing the symmetry-preserving residual interaction associated with a given mean-field potential, it is shown that the original Marshalek formulation can be recovered with a slight modification. Furthermore, the strength of this residual interaction is uniquely determined for a given mean-field so that there is no new parameter in the calculation of the RPA step, i.e., the theory always has the

consistency between the mean-field and the residual interaction.

As a mean-field, in the present work, we have used the new Woods-Saxon potential that gives correct density distributions for both protons and neutrons. It is believed to give better descriptions than, e.g., the Nilsson potential, which was employed in the previous works.[46)–48)] It has been found that the RPA solutions, which can be interpreted as wobbling excitations, exist systematically in the Lu and Hf region, if the proper mean-field parameters are adopted, i.e., the pronounced triaxial deformation or the triaxially superdeformed (TSD) shape. The general features of the calculated RPA solutions are rather similar to those obtained in the previous works employing the Nilsson potential, except for the $B(M1)$ ratio that is too large, and the stability against the change of the mean-field parameters are demonstrated in detail. It should be emphasized that the obtained RPA solutions satisfy the properties expected from the rotor model; especially the large out-of-band $B(E2)$ is reproduced if the same triaxial deformation as the particle-rotor model analysis[22)–25)] is used. All these results confirm the wobbling excitations in the TSD bands from the microscopic view point.

We must admit that the results of our calculations do not agree very well with the experimental data of the Lu isotopes. The excitation energies of the wobbling excitation are underestimated about 150−200 keV, which may suggest that the particle-rotor coupling effect is not fully taken into account. We obtain the similar excitation energies for wobbling mode in the even-even Hf nuclei. Therefore, it is crucial to observe the wobbling excitations in even-even nuclei to draw a definite conclusion for whether the effect of the particle-rotor coupling is essential for the wobbling excitation observed in the odd-Z Lu isotopes. As for the out-of-band to in-band $B(E2)$ ratio, the calculated results decrease as functions of the rotational frequency just like in the rotor model, if the deformation parameters are kept constants. The measured $B(E2)$ ratio in ^{163}Lu is almost constant, and one has to increase the triaxiality parameter considerably as a function of the rotational frequency in order to reproduce this behavior. However, the Nilsson Strutinsky calculation gives almost constant triaxial deformation and the obtained triaxiality is too small to account for the average magnitude of the $B(E2)$ ratio. The better microscopic description of the wobbling motion is certainly a challenge to the existing microscopic theory.

Acknowledgements

We are deeply indebted to Ramon Wyss for providing us with the new parameter set of the Woods-Saxon potential, which makes us possible to perform the present work.

References

1) S. W. Ødegård et al., Phys. Rev. Lett. **86** (2001), 5866.
2) D. R. Jensen et al., Phys. Rev. Lett. **89** (2002), 142503.
3) I. Hamamoto et al., Acta Phys. Pol. B **32** (2001), 2545.
4) G. B. Hagemann, Eur. Phys. J. A **20** (2004), 183.
5) A. Bohr and B. R. Mottelson, *Nuclear Structure*, vol. II (Benjamin, New York, 1975).
6) D. R. Jensen et al., Nucl. Phys. A **703** (2002), 3.

7) D. R. Jensen et al., Eur. Phys. J. A **19** (2004), 173.
8) G. Schönwaßer et al., Phys. Lett. B **552** (2003), 9.
9) H. Amro et al., Phys. Lett. B **553** (2003), 197.
10) P. Bringel et al., Eur. Phys. J. A **24** (2005), 167.
11) I. Ragnarsson, Phys. Rev. Lett. **62** (1989), 2084.
12) S. Åberg, Nucl. Phys. A **520** (1990), 35.
13) R. Bengtsson and H. Ryde, Eur. Phys. J. A **22** (2004), 355.
14) R. Bengtsson, `http://www.matfys.lth.se/~ragnar/TSD.html`
15) G. Schönwaßer et al., Eur. Phys. J. A **15** (2002), 435.
16) A. Görgen et al., Phys. Rev. C **69** (2004), 031301.
17) H. Amro et al., Phys. Lett. B **506** (2001), 39.
18) A. Neußer et al., Eur. Phys. J. A **15** (2002), 439.
19) A. Neußer-Neffgen et al., Phys. Rev. C **73** (2006), 034309.
20) Y. C. Zhang et al., Phys. Rev. C **76** (2007), 064321.
21) D. Hartley et al., Phys. Lett. B **608** (2005), 31.
22) I. Hamamoto, Phys. Rev. C **65** (2002), 044305.
23) I. Hamamoto and G. B. Hagemann, Phys. Rev. C **67** (2003), 014319.
24) K. Tanabe and K. Sugawara-Tanabe, Phys. Rev. C **73** (2006), 034305.
25) K. Tanabe and K. Sugawara-Tanabe, Phys. Rev. C **77** (2008), 064318.
26) S. G. Nilsson and I. Ragnarsson, *Shapes and Shells in Nuclear Structure* (Cambridge University Press, 1995).
27) P. Ring and P. Schuck, *The Nuclear Many-Body Problem* (Springer-Verlag, 1980).
28) F. Villars and G. Cooper, Ann. of Phys. **56** (1970), 224.
29) D. R. Bes and J. Kurchan, *The treatment of collective coordinates in many-body systems*, *Lecture Notes in Phys.* Vol. 34 (World Scientific, Singapore, 1990).
30) J. Kurchan, D. R. Bes and S. C. Barrios, Nucl. Phys. A **509** (1990), 306.
31) J. P. Garrahan and D. R. Bes, Nucl. Phys. A **573** (1994), 448.
32) E. R. Marshalek, Nucl. Phys. A **331** (1979), 429.
33) D. Janssen and I. N. Mikhailov, Nucl. Phys. A **318** (1979), 390.
34) V. G. Zelevinsky, Nucl. Phys. A **344** (1980), 109.
35) A. K. Kerman and N. Onishi, Nucl. Phys. A **361** (1981), 179.
36) N. Onishi, Nucl. Phys. A **456** (1986), 279.
37) K. Kaneko, Phys. Rev. C **45** (1992), 2754.
38) K. Kaneko, Phys. Rev. C **49** (1994), 3014.
39) T. Marumori, T. Maskawa, F. Sakata and A. Kuriyama, Prog. Theor. Phys. **64** (1980), 1294.
40) M. Yamamura and A. Kuriyama, Prog. Theor. Phys. Suppl. No. 93 (1987), 1.
41) L. D. Landau and E. M. Lifshitz, *Mechanics* (Pergamon, London, 1960).
42) Y. R. Shimizu and M. Matsuzaki, Nucl. Phys. A **588** (1995), 559.
43) E. R. Marshalek, Nucl. Phys. A **275** (1977), 416.
44) J. L. Egido, H. J. Mang and P. Ring, Nucl. Phys. A **339** (1980), 390.
45) Y. R. Shimizu and K. Matsuyanagi, Prog. Theor. Phys. **70** (1983), 144.
46) M. Matsuzaki, Y. R. Shimizu and K. Matsuyanagi, Phys. Rev. C **65** (2002), 041303.
47) M. Matsuzaki, Y. R. Shimizu and K. Matsuyanagi, Eur. Phys. J. A **20** (2004), 189.
48) M. Matsuzaki, Y. R. Shimizu and K. Matsuyanagi, Phys. Rev. C **69** (2004), 034325.
49) D. Almehed, R. G. Nazmitdinov and F. Dönau, Physica Scripta **T125** (2006), 139.
50) M. Matsuzaki, Nucl. Phys. A **509** (1990), 269.
51) J. Kvasil and R. G. Nazmitdinov, Phys. Lett. B **650** (2007), 331.
52) S. Frauendorf, Rev. Mod. Phys. **73** (2001), 463.
53) M. Matsuzaki and S.-I. Ohtsubo, Phys. Rev. C **69** (2004), 064317.
54) M. Matsuzaki, Prog. Theor. Phys. **119** (2008), 421.
55) Y. R. Shimizu, T. Shoji and M. Matsuzaki, Phys. Rev. C **77** (2008), 024319.
56) G. Andersson, S. E. Larsson, G. Leander, P. Möller, S. G. Nilsson, I. Ragnarsson, S. Åberg, J. Dudek, B. Nerlo-Pomorska, K. Pomorski and Z. Szymański, Nucl. Phys. A **268** (1976), 205.
57) S. Kinouchi, Ph.D. thesis, University of Tsukuba, 1988.
58) T. Nakatsukasa, K. Matsuyanagi, S. Mizutori and Y. R. Shimizu, Phys. Rev. C **53** (1996), 2213.

59) J. Kvasil and R. G. Nazmitdinov, Phys. Rev. C **73** (2006), 014312.
60) T. Shoji and Y. R. Shimizu, Int. J. Mod. Phys. E **15** (2006), 1407.
61) J. Dudek, A. Majhofer, J. Skalski, T. Werner, S. Cwiok and W. Nazarewicz, J. of Phys. G **5** (1979), 1359.
62) S. G. Rohozinski and A. Sobiczewski, Acta Phys. Pol. B **12** (1981), 1001.
63) W. Nazarewicz and A. Sobiczewski, Nucl. Phys. A **369** (1981), 396.
64) R. Wyss, private communication.
65) Y. R. Shimizu, M. Matsuzaki and K. Matsuyanagi, Phys. Rev. C **72** (2005), 014306.
66) N. I. Pyatov and D. I. Salamov, Nukleonika **22** (1977), 127.
67) A. Bohr and B. R. Mottelson, *Nuclear Structure*, vol. I (Benjamin, New York, 1969).
68) P. A. M. Dirac, *Lectures in Quantum Mechanics* (Yeshiva University Press, New York, 1964).
69) T. Kishimoto et al., Phys. Rev. Lett. **35** (1975), 552.
70) H. Sakamoto and T. Kishimoto, Nucl. Phys. A **501** (1989), 205.
71) T. Suzuki and D. J. Rowe, Nucl. Phys. A **289** (1977), 461.
72) E. R. Marshalek, Phys. Rev. C **29** (1984), 640.
73) S. Cwiok, J. Dudek, W. Nazarewicz, J. Skalski and T. Werner, Comput. Phys. Commun. **46** (1987), 379.
74) Y. R. Shimizu, E. Vigezzi and R. A. Broglia, Nucl. Phys. A **509** (1990), 80.
75) T. Bengtsson and I. Ragnarsson, Nucl. Phys. A **436** (1985), 14.
76) R. Bengtsson and S. Frauendorf, Nucl. Phys. A **327** (1979), 139.
77) M. Matsuzaki, Y. R. Shimizu and K. Matsuyanagi, Prog. Theor. Phys. **79** (1988), 836.
78) G. Audi and A. H. Wapstra, Nucl. Phys. A **595** (1995), 409.
79) R. Wyss, W. Satula, W. Nazarewicz and A. Johnson, Nucl. Phys. A **511** (1990), 324.